JOURNAL OF GEOPHYSICAL RESEARCH: ATMOSPHERES, VOL. 118, 9233–9257, doi:10.1002/jgrd.50530, 2013

Organic aerosol composition and sources in Pasadena, California, during the 2010 CalNex campaign

P. L. Hayes,[1,2] A. M. Ortega,[1,3] M. J. Cubison,[1,2] K. D. Froyd,[1,4] Y. Zhao,[5] S. S. Cliff,[5] W. W. Hu,[1,6] D. W. Toohey,[3] J. H. Flynn,[7] B. L. Lefer,[7] N. Grossberg,[7] S. Alvarez,[7] B. Rappenglück,[7] J. W. Taylor,[8] J. D. Allan,[8,9] J. S. Holloway,[1,4] J. B. Gilman,[1,4] W. C. Kuster,[4] J. A. de Gouw,[1,4] P. Massoli,[10] X. Zhang,[11] J. Liu,[11] R. J. Weber,[11] A. L. Corrigan,[12] L. M. Russell,[12] G. Isaacman,[13] D. R. Worton,[13,14] N. M. Kreisberg,[14] A. H. Goldstein,[13] R. Thalman,[1,2] E. M. Waxman,[1,2] R. Volkamer,[1,2] Y. H. Lin,[15] J. D. Surratt,[15] T. E. Kleindienst,[16] J. H. Offenberg,[16] S. Dusanter,[17,18,19] S. Griffith,[17] P. S. Stevens,[17] J. Brioude,[1,4] W. M. Angevine,[1,4] and J. L. Jimenez[1,2]

Received 23 October 2012; revised 19 May 2013; accepted 25 May 2013; published 29 August 2013.

[1] Organic aerosols (OA) in Pasadena are characterized using multiple measurements from the California Research at the Nexus of Air Quality and Climate Change (CalNex) campaign. Five OA components are identified using positive matrix factorization including hydrocarbon-like OA (HOA) and two types of oxygenated OA (OOA). The Pasadena OA elemental composition when plotted as H : C versus O : C follows a line less steep than that observed for Riverside, CA. The OOA components from both locations follow a common line, however, indicating similar secondary organic aerosol (SOA) oxidation chemistry at the two sites such as fragmentation reactions leading to acid formation. In addition to the similar evolution of elemental composition, the dependence of SOA concentration on photochemical age displays quantitatively the same trends across several North American urban sites. First, the OA/ΔCO values for Pasadena increase with photochemical age exhibiting a slope identical to or slightly higher than those for Mexico City and the northeastern United States. Second, the ratios of OOA to odd-oxygen (a photochemical oxidation marker) for Pasadena, Mexico City, and Riverside are similar, suggesting a proportional relationship between SOA and odd-oxygen formation rates. Weekly cycles of the OA components are examined as well. HOA exhibits lower concentrations on Sundays versus weekdays, and the decrease in HOA matches that predicted for primary vehicle emissions using fuel sales data, traffic counts, and vehicle emission ratios. OOA does not display a weekly cycle—after accounting for differences in photochemical aging —which suggests the dominance of gasoline emissions in SOA formation under the assumption that most urban SOA precursors are from motor vehicles.

Citation: Hayes, P. L., et al. (2013), Organic aerosol composition and sources in Pasadena, California during the 2010 CalNex campaign, *J. Geophys. Res. Atmos.*, *118*, 9233–9257, doi:10.1002/jgrd.50530.

Additional supporting information may be found in the online version of this article.

[1]Cooperative Institute for Research in the Environmental Sciences, University of Colorado Boulder, Boulder, Colorado, USA.
[2]Department of Chemistry and Biochemistry, University of Colorado Boulder, Boulder, Colorado, USA.
[3]Department of Atmospheric and Oceanic Sciences, University of Colorado Boulder, Boulder, Colorado, USA.
[4]NOAA Chemical Sciences Division, Boulder, Colorado, USA.
[5]Air Quality Research Center, University of California, Davis, California, USA.
[6]College of Environmental Sciences and Engineering, Peking University, Beijing, China.
[7]Department of Earth and Atmospheric Sciences, University of Houston, Houston, Texas, USA.

Corresponding author: J. L. Jimenez, Cooperative Institute for Research in the Environmental Sciences, University of Colorado Boulder, Boulder, CO 80309, USA. (jose.jimenez@colorado.edu)

2169-897X/13/10.1002/jgrd.50530

[8]School of Earth, Atmospheric, and Environmental Sciences, University of Manchester, Manchester, UK.
[9]National Centre for Atmospheric Science, University of Manchester, Manchester, UK.
[10]Aerodyne Research Inc., Billerica, Massachusetts, USA.
[11]Georgia Institute of Technology, Atlanta, Georgia, USA.
[12]Scripps Institution of Oceanography, University of California, San Diego, La Jolla, California, USA.
[13]Department of Environmental Science, Policy and Management, University of California, Berkeley, California, USA.
[14]Aerosol Dynamics Inc., Berkeley, California, USA.
[15]Department of Environmental Sciences and Engineering, University of North Carolina at Chapel Hill, Chapel Hill, North Carolina, USA.
[16]U.S. Environmental Protection Agency, Research Triangle Park, North Carolina, USA.
[17]Center for Research in Environmental Science, School of Public and Environmental Affairs, and Department of Chemistry, Indiana University, Bloomington, Indiana, USA.
[18]Université Lille Nord de France, Lille, France.
[19]EMDouai, Douai, France.

1. Introduction

[2] Atmospheric aerosols have been the subject of intensive ongoing research due to their important impacts on the radiative forcing of climate, which occur through several mechanisms that include the scattering and absorption of solar radiation as well as the alteration of the formation and properties of clouds [*International Panel on Climate Change*, 2007]. In addition, atmospheric aerosols reduce visibility [*Watson*, 2002] and increase cardiac and respiratory disease in humans [*Dockery and Pope*, 1994; *Dockery et al*., 1993]. The impact of aerosols on climate, the environment, and human health is determined, in part, by particle size and chemical composition. In many environments, a large fraction (~50%) of the submicron aerosol mass in the troposphere is organic aerosol (OA), but the sources, composition, and chemical processing of OA are not well understood [*Jimenez et al*., 2009]. Generally, OA is comprised of thousands of individual compounds that are either directly emitted into the atmosphere (i.e., "primary" OA or "POA") or formed though chemical reactions involving gas phase precursors (i.e., "secondary" OA or "SOA"). The multiple sources and complexity of molecular composition represent major challenges for understanding and prediction of OA properties.

[3] Elevated aerosol concentrations are often associated with megacities such as Los Angeles (LA). Particulate matter concentrations in LA are among the highest in the United States (American Lung Association, State of the air, 2011, http://www.stateoftheair.org/), and multiple previous measurement campaigns have aimed to characterize aerosols in this region. These campaigns include the 1987 Southern California Air Quality Study [*Lawson*, 1990], the 1997 Southern California Ozone Study (SCOS97-NARSTO) [*Croes and Fujita*, 2003], the Study of Organic Aerosol at Riverside, which took place in the summer (SOAR-1) and fall (SOAR-2) of 2005 [*Docherty et al*., 2011], and the 2009 Pasadena Aerosol Characterization Observatory (PACO) [*Hersey et al*., 2011]. In addition, several research flights were performed over California and LA during the Arctic Research of the Composition of the Troposphere from Aircraft and Satellites Campaign (ARCTAS-CARB) [*Jacob et al*., 2010]. Using data from these campaigns, it has been shown that SOA represents a majority of the total OA mass in both Riverside [*Docherty et al*., 2008] and Pasadena, CA [*Hersey et al*., 2011], which is similar to findings in other urban regions [*Jimenez et al*., 2009]. The gas phase precursors for SOA potentially have many sources including vehicle emissions, the biosphere, biomass burning, and food cooking [*Bahreini et al*., 2012; *Hodzic et al*., 2010; *Schauer et al*., 1999, 2002b]. Also, vehicle emissions, food cooking, biomass burning, and primary biogenics have all been identified as sources of POA in the South Coast Air Basin [*Williams et al*., 2010; *Wonaschutz et al*., 2011].

[4] The California Research at the Nexus of Air Quality and Climate Change (CalNex) field campaign was conducted in 2010 and was a multi-institution effort to address outstanding questions regarding atmospheric chemistry processes over the state of California and the adjacent Pacific coastal region [*Ryerson et al.*, 2013]. The CalNex campaign featured several research aircraft, the research vessel Atlantis off the California coast, and two ground sites in Pasadena and Bakersfield. A major scientific goal for CalNex was to improve scientific understanding of atmospheric aerosols in California and, specifically, to characterize important SOA precursors and formation pathways, as well as the impacts of aerosols on radiative forcing and cloud formation [*National Oceanic and Atmospheric Administration*, 2008]. For CalNex, the Pasadena ground site was uniquely equipped to characterize aerosols and, especially, organic aerosols. In total, approximately 70 gas and particle phase measurements were taken at the site representing, to our knowledge, one of the largest studies of aerosols and their precursors. A full list of the instrumentation is available in the CalNex overview [*Ryerson et al.*, 2013] and also at http://tinyurl.com/CalNex. Additionally, the ground site featured many state-of-the-art aerosol instruments including several that had never been field-deployed previously.

[5] Here we present a detailed analysis of aerosol measurements from multiple instruments, including online and off-line bulk and single particle methods, deployed to the Pasadena ground site during CalNex. The goals of this work are to quantitatively evaluate SOA formation for the South Coast Air Basin and compare it against other major urban regions, as well as to determine the contributions of various sources to organic aerosol mass loadings. In particular, the relative importance of diesel versus gasoline emissions in secondary organic aerosol formation has been a source of scientific controversy [*Bahreini et al*., 2012; *Gentner et al*., 2012] and will be examined here. To achieve these goals, the following approach is utilized: (1) using positive matrix factorization (PMF), the components of OA are identified and characterized (section 3.2); (2) the POA emission ratios with elemental carbon (EC) and CO are determined and rationalized (section 3.3); (3) the dependence of SOA concentration on photochemical age is quantified and compared against previous measurements conducted in Riverside, Mexico City, and the northeastern United States (section 3.4); and (4) the weekly cycles (or lack thereof) in POA and SOA concentrations are analyzed in the context of understanding the relative contributions to each from diesel and gasoline motor vehicles (section 3.5). The unique findings of this work include the observation of a similar SOA formation rate for Pasadena versus other urban locations, the first reported weekly cycle for POA concentrations, and an improved analysis of the contribution of diesel emissions to SOA formation based on the lack of a weekly cycle in SOA concentrations.

2. Experimental

2.1. CalNex Ground Site in Pasadena, CA

[6] The CalNex Pasadena ground site was located on the California Institute of Technology (Caltech) campus in Pasadena, CA (34.1406 N, 118.1225 W, 236 m above mean sea level). The measurement period was 15 May 2010 00:00 to 16 June 2010 00:00 (local time). The Pasadena ground site was located 18 km northeast of downtown Los Angeles. Pasadena lies within the South Coast Air Basin, which is bordered on the north and east by the San Gabriel, San Bernardino, and San Jacinto mountains as well as on the southwest by the Pacific Ocean. Pasadena is part of the dense, urban Los Angeles metropolitan area. The prevailing wind direction during daytime in Pasadena was from

the southwest due to the sea breeze, which brought air masses from the Santa Monica and San Pedro Bays through central Los Angeles to Pasadena (FLEXPART back trajectories are available in section A of the supporting information). At nighttime, winds were weaker and were most frequently from the southwest or southeast. Sunrise and sunset were approximately 05:30 and 20:00 (local time) during the sampling period. Boundary layer height, temperature, and relative humidity (RH) data are presented in section A of the supporting information.

2.2. AMS Sampling and Analysis

[7] The concentrations of submicron nonrefractory ($nrPM_1$) organic and inorganic (nitrate, sulfate, ammonium, chloride) aerosol particles were measured using an Aerodyne High-Resolution Time-of-Flight Aerosol Mass Spectrometer (hereinafter referred to as "AMS") [*DeCarlo et al*., 2006]. The AMS sampled from an inlet equipped with a $PM_{2.5}$ cyclone located 2 m above the roof of the container housing the instrument. The sampled air passed through a 6.8 m insulated copper inlet line and a dryer prior to analysis by the AMS. The resulting data were averaged over 2.5 min intervals. The ion paths through the time-of-flight chamber were alternated between "V" and "W" modes every 150 s, and the reported concentrations correspond to V-mode acquisition periods only. Size distributions were acquired during every V-mode acquisition by operating the AMS in particle time-of-flight mode [*Jimenez et al*., 2003]. All data were analyzed using standard AMS software (SQUIRREL v1.51 and PIKA v1.10) within Igor Pro 6.2.1 (WaveMetrics, Lake Oswego, OR) (D. Sueper, ToF-AMS Analysis Software, 2011, http://cires.colorado.edu/jimenez-group/wiki/index.php/ToF-AMS_ Analysis_Software).

[8] It is well known that for most ambient sampling conditions, a collection efficiency (CE) correction must be applied to the AMS data to account for particle bounce from the AMS vaporizer [*Middlebrook et al*., 2012]. Mass concentrations are typically calculated with a default CE of 0.5. The degree to which particles bounce, and hence collection efficiency, is a function of particle phase, which is influenced by the relative humidity of the sampling line, the acidity/neutralization of the sulfate content, the ammonium nitrate content, and the organic liquid content [*Middlebrook et al*., 2012]. The sample flow was dried as described above, and the sulfate content was largely neutralized (see Appendix). Thus, these experimental parameters are not expected to impact CE. Ammonium nitrate concentrations varied widely during the measurement period though, and accordingly, a nitrate-dependent CE is applied following *Nemitz* [2010]. Quantifying the organic liquid content is challenging for ambient samples; however, the ratio of AMS mass to Scanning Mobility Particle Sizer (SMPS) mass exhibits no dependence on the amount of OA oxidation as measured by O : C indicating that phase changes associated with organic material are either not occurring or are not influencing the particle bounce and CE. In total, the aerosol mass concentrations measured by the AMS after applying the CE correction, which ranged from 0.5 to 0.7, are consistent with most other measurements from the Pasadena ground site. The relevant intercomparisons are discussed in section B of the supporting information for this paper, including details regarding how mass concentrations are calculated from SMPS number distributions.

[9] High-resolution (HR) analysis of the mass spectra, including application of the HR AMS fragmentation table, was carried out following previously published procedures [*Aiken et al*., 2007, 2008]. The reported AMS mass concentrations were determined from the HR AMS spectra and are very similar to unit mass resolution (UMR) concentrations, within 5%, that are determined using the UMR fragmentation table of *Allan et al*. [2004]. The HR fragmentation table was also used to obtain the OA mass spectral matrix for the PMF analysis described in the next paragraph.

[10] The OA mass spectral matrix was deconvolved into components using PMF, a receptor-based factorization model [*Paatero and Tapper*, 1994]. The application of PMF to AMS spectra has been discussed in detail previously [*Ulbrich et al*., 2009; *Zhang et al*., 2011]. The same method is used here including the PMF2 algorithm, which is run in robust mode via the PMF Evaluation Tool panel (v2.03). The high-resolution organic aerosol mass spectra for the entire CalNex campaign were analyzed, and the full range of the high-resolution spectra was utilized (m/z 12–204). Error matrices were calculated using the methods of *Allan et al*. [2003] and *Ulbrich et al*. [2009]. Weak variables (i.e., m/z's) with lower signal-to-noise ratios ($0.2 < S/N < 2$) were down-weighted by a factor of 3, and bad variables ($S/N \leq 0.2$) were down-weighted by a factor of 10 following the recommendations of *Paatero and Hopke* [2003]. For the results presented here, the model error was set to zero.

2.3. Colocated CalNex Measurements Utilized in This Study

[11] A SMPS (Model 3936, TSI Inc.) measured ambient number distributions between 7 and 690 nm mobility diameter. The SMPS was operated at a sampling frequency of 5 min and used the same inlet as the AMS (including drier) except that the aerosol flow passed through an additional 2.1 m of copper inlet line (0.3 lpm flow). For the SMPS, the aerosol flow rate was 0.3 lpm and the sheath flow rate was 3 lpm. Ambient particle number distributions were also measured from 60 to 1000 nm using an Ultra-High Sensitivity Aerosol Spectrometer (Droplet Measurement Technologies), which also used the same inlet as the AMS (including drier), but the sample flow passed through an additional 2 m of inlet line (0.3 lpm flow). A White-Light Optical Particle Counter (WLOPC; Climet model 208 fitted with a multichannel analyzer) measured size distributions from 500 to 4000 nm. Hourly $PM_{2.5}$ organic carbon (OC) and elemental carbon (EC) concentrations were measured using a Sunset Labs field OC/EC analyzer [*Peltier et al*., 2007]. Blank-corrected optical OC and EC data from the Sunset field analyzer are reported here. Measurements of refractory black carbon (rBC) were performed with a Single Particle Soot Photometer (Droplet Measurement Technologies) [*Schwarz et al*., 2006], as well as with a Soot Particle Aerosol Mass Spectrometer (SP-AMS; Aerodyne Research and Droplet Measurement Technology) [*Onasch et al*., 2012]. The concentrations of semivolatile and particulate organic molecular tracers were measured by 2-D Thermal Desorption Aerosol Gas Chromatography Mass Spectrometry (2DTAG; UC-Berkeley and Aerosol Dynamics) [*Worton et al*., 2012]. $PM_{2.5}$ nitrate and sulfate concentrations were measured with a Particle-Into-Liquid Sampling and Ion Chromatography (PILS-IC) system [*Orsini et al*., 2003]. The Particle Analysis by Laser

Mass Spectrometry (PALMS) instrument provided number fractions for individual particle composition classes from 190 to 4000 nm [*Froyd et al*., 2009; *Thomson et al*., 2000]. The PALMS instrument also measures scattered light from single particles allowing for calculation of particle size in addition to particle classification. Volume concentrations of the different PALMS particle classes were calculated by multiplying the volume concentration size distribution determined from the SMPS or WLOPC measurements by the fractions of the different PALMS particle types in each size bin. Particle optical extinction for PM_1 was measured at 532 nm and 630 nm by a Cavity Attenuated Phase Shift instrument [*Kebabian et al*., 2007; *Massoli et al*., 2010]. All of the online measurements described in this paragraph were located at the CalNex ground site described above.

[12] Data from offline particulate matter measurements are included in this paper as well. In particular, size-resolved elemental concentrations were determined by X-ray fluorescence (XRF) analysis of Mylar substrates from a rotating drum impactor. The XRF analysis was performed at the Advanced Light Source at Lawrence Berkeley National Lab. Using the XRF results, the mineral dust concentration corresponding to oxides of Al, Si, Ca, K, Fe, and Ti is estimated from the elemental concentrations following the method of *Simon et al*. [2011] and *Malm et al*. [1994]. The particulate metal concentration is calculated as the sum of the mass concentrations of Mg, V, Cr, Mn, Co, Ni, Cu, Zn, Ga, As, Se, Rb, Sr, Y, Zr, Mo, and Pb. The Cl concentrations from XRF measurements are reported as refractory chloride (rCl), since the placement of samples under vacuum for analysis is expected to cause evaporation of nonrefractory species such ammonium chloride. The time resolution of the XRF data was 1.5 h. Offline OC measurements of high-volume $PM_{2.5}$ samples collected with quartz fiber filters were performed using three separate sets of filters and two laboratory-based Sunset Labs OC/EC analyzers (NIOSH TOT protocol). For clarity, the three sets of filters are named according to the institution that collected them: Georgia Institute of Technology (GIT), U.S. Environmental Protection Agency (EPA), and University of North Carolina (UNC). Following the technique of *Russell et al*. [2009], Fourier transform infrared (FTIR) spectroscopy analysis of Teflon filter samples provided $PM_{2.5}$ OA and organic functional group mass concentrations. All samples for offline analyses were collected at about 12 m above ground level on the roof of the Keck Building located on the Caltech campus approximately 0.3 km southwest of the ground site.

[13] The concentration of O_3 was measured by UV differential absorption (49c Ozone Analyzer, Thermo Scientific), and CO concentrations were measured by two vacuum-UV resonance fluorescence instruments (AL5001 and AL5002, Aerolaser) [*Gerbig et al*., 1999]. An in situ Gas Chromatography Mass Spectrometry (GC-MS) instrument provided the mixing ratios for a variety of VOCs [*Gilman et al*., 2009]. A fluorescence assay by gas expansion instrument was utilized to determine the OH concentration [*Dusanter et al*., 2009]. The NO_x and NO_y concentrations were measured using chemiluminescence (42i-TL with Mo converter, Thermo Scientific), and NO_2 was measured with Cavity-Enhanced Differential Optical Absorption Spectroscopy (CE-DOAS) [*Thalman and Volkamer*, 2010]. The CE-DOAS instrument was located on the Caltech Millikan Library roof, which is approximately 45 m tall and 0.5 km southwest of the Pasadena ground site.

[14] Meteorological data were acquired by a station that included a temperature/RH sensor (Campbell Scientific Inc., HMP35C) and a wind monitor (R.M. Young, 05103). The boundary layer height was determined using a ceilometer (Vaisala, CL31) following the method described by *Haman et al*. [2012], and the ceilometer results have been shown to be consistent with boundary layer heights from Weather Research Forecasting (WRF) modeling [*Washenfelder et al*., 2011]. To track the origins of the air masses sampled at the ground site, a modified version of the FLEXPART Lagrangian particle dispersion model [*Stohl et al*., 2005] was used to calculate back trajectories of air masses based on advection and turbulent mixing processes. The main modification consists of using time-averaged winds from the WRF (version 3.3) meteorology model instead of instantaneous winds to improve uncertainties within the FLEXPART model [*Brioude et al*., 2012]. The WRF output has a spatial grid of 4 km × 4 km, with a temporal resolution of 30 min and 60 vertical levels. Lastly, all linear regressions in this paper are performed as orthogonal distance regressions (ODR) using Igor Pro 6.2.1 software.

3. Results and Discussion

3.1. Total Submicron Aerosol Composition at the Pasadena Ground Site During CalNex

[15] While the focus of this paper is OA, a survey of the total aerosol composition can provide valuable context for the OA analysis, and providing such a context is the goal of this section (3.1). (Note: Comparisons with previous campaigns as well as additional figures regarding the total submicron aerosol composition are shown in section C of the supporting information.) The time series for the $nrPM_1$ species and EC are shown in Figure 1b. In addition, the diurnal cycles of the $nrPM_1$ species and EC are shown in Figure 2a. The time series for metals, mineral dust, and refractory chloride (rCl) are shown in Figure 1c, and for comparison, the PALMS particle type time series are included in Figure 1 as well (Figures 1d and 1e). The fractional composition of the total submicron mass is determined by combining the AMS, Sunset Analyzer, XRF, and PALMS measurements, and is summarized in Figure 2c. (Note: See Figure 2 caption for details regarding which instrument measured each species as well as how the PALMS data are converted to mass concentration.) In the interpretation of the data in Figures 1 and 2, it is important to consider some differences in size cuts of the measurements. First, the XRF measurements used in Figures 1 and 2 correspond to a size cut of 1150 nm aerodynamic diameter. By linearly interpolating the size-resolved XRF measurements, the average overestimate relative to the actual PM_1 concentrations was found to be approximately 30%. Second, the online Sunset OC/EC analyzer was equipped with a $PM_{2.5}$ cyclone for most of the campaign. From 12 to 16 June, the EC measurement was performed while switching between $PM_{2.5}$ and PM_1 cyclones, and the ratio of the PM_1 EC to the linearly interpolated $PM_{2.5}$ EC was 0.93 (±0.19 standard deviation). Thus, while the EC data in Figures 1 and 2 may overestimate the true PM_1 EC concentrations, it is expected that this error will be reasonably small (~7%). Despite these overestimates of refractory mass, the total

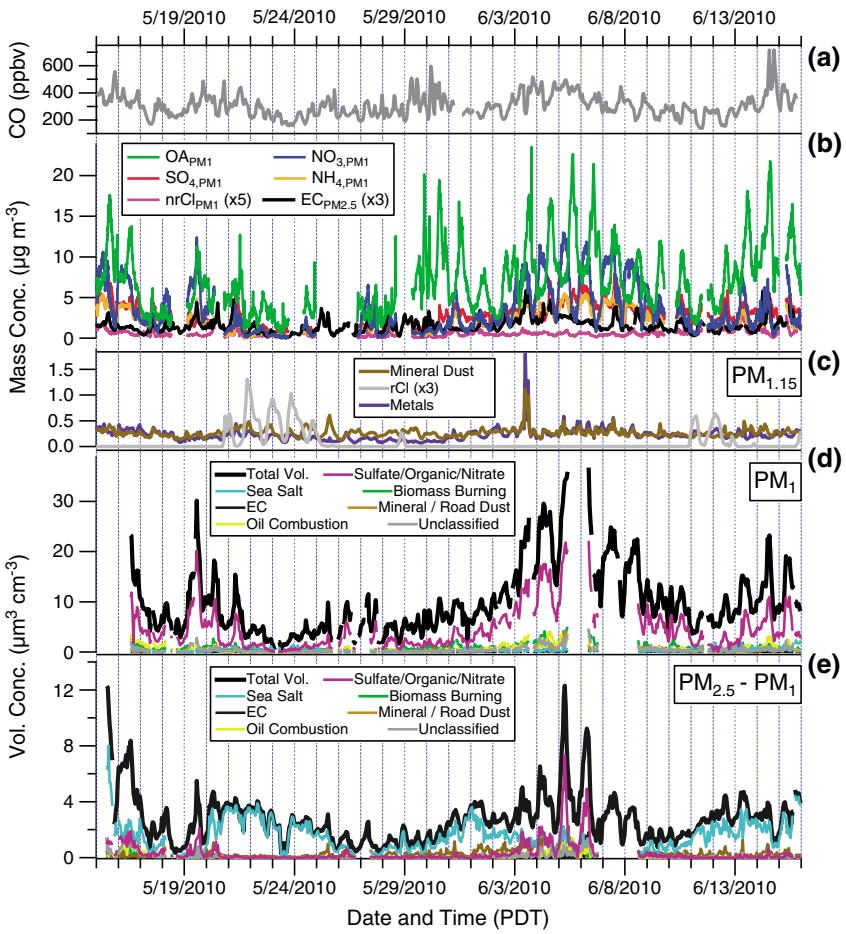

Figure 1. (a) CO concentration. (b) The nonrefractory aerosol concentrations sampled by the AMS. The measured species are organics (OA), nitrate (NO_3), sulfate (SO_4), ammonium (NH_4), and nonrefractory chloride (nrCl). The elemental carbon (EC) concentration was measured in situ by a Sunset analyzer. For completeness, the EC data include occasional periods when a PM_1 cyclone was used instead of a $PM_{2.5}$ cyclone (12–16 June). (c) Refractory aerosol mass concentrations as measured by XRF (rCl: refractory chloride). Particle type volume concentrations measured by the PALMS for (d) PM_1 and (e) for particles between 1 and 2.5 μm diameters. All size cuts are aerodynamic diameters, and the PALMS data have been converted from geometric diameters (1 μm aerodynamic diameter = 0.784 μm geometric diameter).

PM_1 concentration is still dominated by nonrefractory species (OA + sulfate + nitrate + ammonium + nrCl) that account for 93% of the measured mass. Similarly, particle types measured by the PALMS instrument that are predominately composed of nonrefractory material comprised 90% of submicron aerosol volume (Figure 3).

[16] A clear diurnal cycle is observed for most $nrPM_1$ species. As shown in Figure 2, the maxima in the EC and CO (commonly used combustion emission tracers) diurnal cycles are both observed between 12:00 and 13:00 PDT (local time). These maxima do not coincide with the Los Angeles County morning rush hour, which occurs between about 06:00 and 08:00 PDT [*Caltrans*, 2010]. Instead, they appear to result from polluted air masses initially emitted in the source-rich regions west and south of Pasadena. The wind speed and wind direction measured at the ground site are consistent with the transport of this plume to Pasadena over several hours. In addition, FLEXPART back trajectories show that the air masses over the Pasadena ground site when EC and CO concentrations are highest have significant footprint residence times over downtown LA as well as the Ports of LA and Long Beach, which are regions with significant combustion emissions.

[17] Compared to EC and CO, the OA concentrations peak later in the day, about 3 pm, which corresponds to the same time of day when air masses over the Pasadena ground site were the most photochemically processed (Figure 2b). The photochemical age for the air mass over the Pasadena site was calculated with two different methods: first, by using the ratio of 1,2,4-trimethylbenzene to benzene, as described in *Parrish et al*. [2007], and second, by defining the photochemical age as $-\log_{10}(NO_x/NO_y)$ similar to *Kleinman et al*. [2008]. All photochemical ages were calculated using a standard OH radical concentration of 1.5×10^6 mol cm^{-3}. For reference, the daily OH radical concentrations averaged for the whole campaign at the Pasadena site was 1.3×10^6 mol cm^{-3}. Interestingly, when using the NO_x/NO_y method, the photochemical age slowly increases from 00:00 to 06:00 local time, likely due to N_2O_5 and $ClNO_2$ formation, which are NO_x sinks [*Chang et al*., 2011]. Outside of this

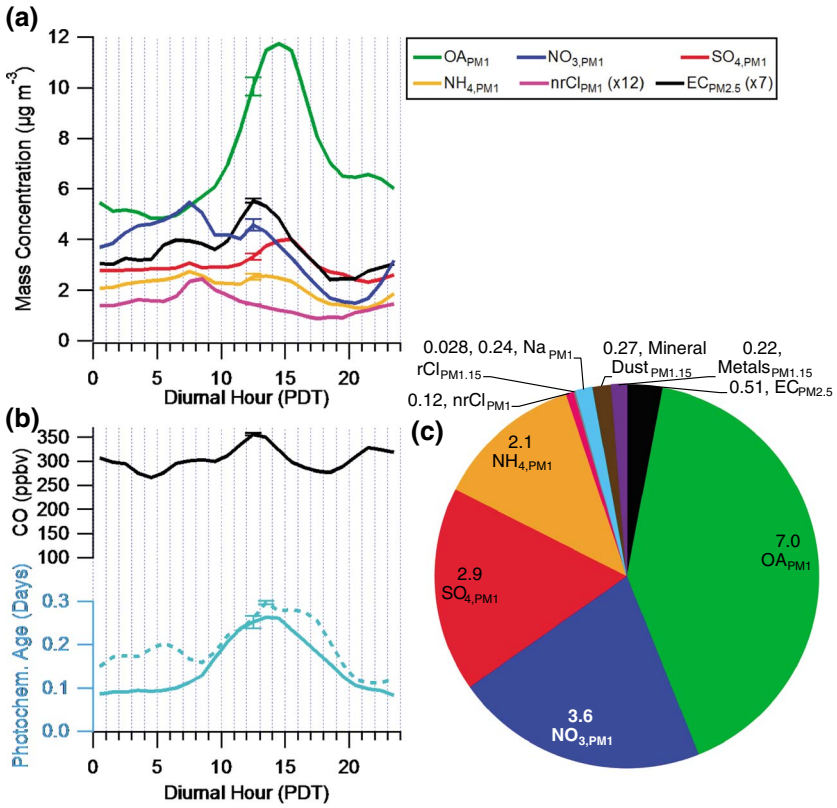

Figure 2. (a) Diurnal profiles for the nonrefractory PM_1 mass concentrations (from AMS) and for EC (from Sunset Analyzer). (b) Diurnal cycles of CO and photochemical age. The photochemical age is determined using the method of *Parrish et al.* [2007] and the ratio of 1,2,4-trimethylbenzene to benzene (solid line), or following *Kleinman et al.* [2008] and defining the photochemical age as $-\log_{10}(NO_x/NO_y)$ (dashed line). (c) Average PM_1 mass concentration (in $\mu g/m^3$) for the ground site (15 May 00:00 to 16 June 00:00) including both refractory and nonrefractory components. Concentrations of mineral dust, metals, and refractory chloride (rCl) were determined from XRF. The sodium concentration is estimated from PALMS sea-salt volume concentrations using a $NaNO_3$ density of 2.1 g cm^{-3} [*Zelenyuk et al.*, 2005] and a sodium to sea-salt mass ratio of 0.308 [*Hall and Wolff*, 1998]. All error bars indicate standard errors of the means.

time range, however, the diurnal cycles of the two photochemical age estimates show good agreement.

[18] The diurnal cycle for OA is relatively flat and low during the early morning hours, 00:00 to 06:00, suggesting a small role for nighttime chemistry driven by either nitrate radicals or aqueous chemistry (RH peaked during this time of day). The lack of aqueous chemistry may be driven by the low oxidant concentrations at night. In parallel work,

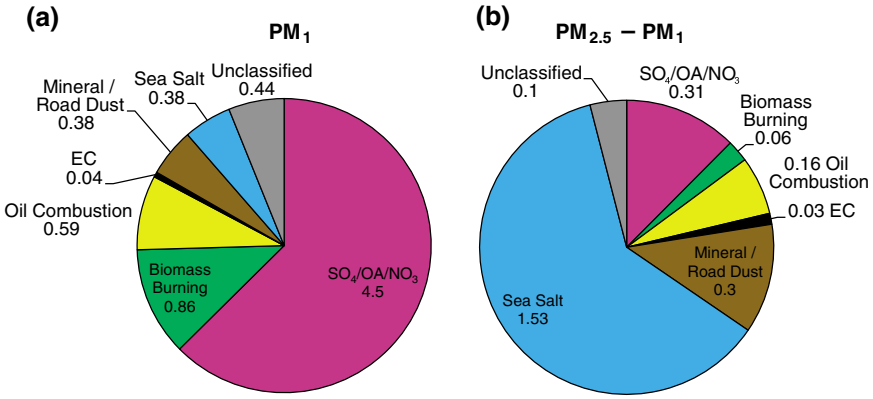

Figure 3. Average volume concentration (in μm^3 cm^{-3}) of the different PALMS particle types for (a) PM_1 and (b) particles between 1 and 2.5 μm diameters at the Pasadena ground site during CalNex. Size ranges correspond to aerodynamic diameters.

Zhang et al. [2012] showed that for Pasadena, the aerosol water was not an important absorbing phase and instead the partitioning coefficient for organics was correlated with OA mass. This result suggests that semivolatile organic compounds are primarily partitioning to the organic phase.

[19] The submicron nitrate diurnal cycle is different from OA with a peak in the morning. The afternoon decrease in nitrate can be attributed to both vertical dilution due to the increase in boundary layer height as well as the higher temperatures and lower RH values that favor evaporation of ammonium nitrate [*Neuman et al*., 2003]. In Pasadena, both nitric acid and ammonia exhibit peaks around noon and elevated concentrations in the afternoon, which is consistent with volatilization of ammonium nitrate [*Veres et al*., 2011; Ellis et al., manuscript in preparation, 2012]. The diurnal cycle of sulfate is not influenced by temperature because ammonium sulfate is nonvolatile at atmospheric temperatures, and the sulfate maximum is observed in the afternoon, which may be due to advection to the ground site from sources west and south of Pasadena and/or photochemical production of sulfate.

[20] In addition to the diurnal cycles, substantial multiday variability is evident in Figure 1. In particular, from 2 to 6 June, there appears to be a high pollution episode where a steady increase in organic aerosol concentrations occurs that is most evident during the nighttime and morning hours. A similar, second high pollution episode is observed at the end of the campaign (13–16 June). These episodes were likely the result of synoptic conditions that trapped pollution in the LA Basin overnight in the boundary layer and in residual layers aloft that tend to contain more aged air [*Lu and Turco*, 1995]. Recirculation of pollution in the LA Basin has been recognized for several decades [e.g., *Blumenthal et al*., 1978; *Moore et al*., 1991; *Ulrickson and Mass*, 1990]. Additionally, a distinct period of greater marine influence is observed between 20 and 25 May. The highest concentrations of rCl are observed during this period, as well as a prominent rCl diurnal cycle (Figure 1c). Dimethyl sulfoxide concentrations, a well-known indicator of marine influence, are also elevated during this period and exhibit a similar diurnal pattern (data not shown).

[21] The PALMS single-particle instrument provides important complementary information regarding aerosol composition at the Pasadena ground site. In particular, the PALMS is capable of characterizing refractory and supermicron aerosols that cannot be measured using the AMS. As stated in the first sentence of this section, the focus of this paper is OA, but a survey of the total aerosol composition can provide valuable context for the OA analysis, hence the inclusion of the PALMS results here. The volume concentration time series for particle composition types identified by the PALMS single-particle instrument are shown in Figures 1d and 1e. In addition, the campaign average volume concentrations are summarized in the pie charts shown in Figures 3a and 3b. The particle composition types were identified from PALMS mass spectra following the method described in *Froyd et al*. [2009]. For instance, biomass burning spectra are identified by a prominent K^+ peak along with organic peaks and a lack of other metals. Vanadium with organic species was used as a tracer to identify aerosol from heavy oil combustion (e.g., from ship engines), which allows for the definition of a particle class termed "Oil Combustion" similar to previous work with other single-particle instruments that studied emissions from commercial ports [*Ault et al*., 2009; *Healy et al*., 2009]. Since the PALMS is a single-particle instrument, it is capable of determining aerosol mixing state. One consideration when comparing the PALMS results against the AMS and other measurements is that the classification of particles typically follows the most abundant components in a particle, but the PALMS volume concentration for each particle type also includes secondary material on the particle that may even dominate the particle volume at the time of detection. For the Pasadena ground site, it was observed that all the particle types contained substantial amounts of nitrate, sulfate, and organics, which indicates that condensation of secondary material is occurring on primary aerosols (e.g., sea salt and mineral dust) and/or particle mixing is occurring through coagulation. The nitrate observed on sea-salt particles is also at least partially due to the heterogeneous reaction between sea salt and nitric acid as discussed in the Appendix. An important conclusion that can be made from the data in Figure 3 is that the PM_1 aerosol volume concentration is dominated by sulfate/OA/nitrate type particles and the supermicron aerosol is dominated by sea-salt particles. These findings are generally consistent with the mass concentration data from XRF and AMS measurements. The PALMS biomass burning results are discussed further in section 3.2.3.

3.2. Source Apportionment of Organic Aerosol Mass by Positive Matrix Factorization

3.2.1. Mass Spectra, Time Series, and Diurnal Cycles of the Organic Aerosol Components

[22] The OA components from the PMF analysis were identified by their mass spectra, diurnal cycles, and elemental composition, as well as by the concentration ratios and correlations of their time series with tracers. Figure 4 shows the mass spectra and time series for the five identified components. Additionally, Figure 5 shows the diurnal profiles of the OA components and the campaign-average fractional contribution of each component to the total OA concentration, as well as a stacked plot illustrating the fractional contributions to OA mass by time of day. A summary of correlations between the OA components and various tracers is provided in section D of the supporting information. The five PMF components identified are (1) hydrocarbon-like organic aerosol (HOA), (2) cooking-influenced organic aerosol (CIOA), (3) local organic aerosol (LOA), (4) semivolatile oxygenated organic aerosol (SV-OOA), and (5) low-volatility oxygenated organic aerosol (LV-OOA). The naming based on volatility is adopted according to several studies showing a relationship between high oxygenation and lower volatility for the OOA components [e.g., *Cappa and Jimenez*, 2010; *Huffman et al*., 2009; *Jimenez et al*., 2009; *Lanz et al*., 2007; *Ulbrich et al*., 2009]. The HOA component has been previously described as a surrogate for primary combustion OA, and the SV-OOA and LV-OOA components as surrogates for "fresher" and "aged" SOA, respectively. [*Aiken et al*., 2008; *Jimenez et al*., 2009; *Ulbrich et al*., 2009; *Zhang et al*., 2007b]. The identification of CIOA is consistent with previous research that has shown food cooking, which includes activities such as seed oil frying and meat charbroiling, is an important source of fine organic aerosol in urban environments [e.g., *Mohr et al*., 2011; *Schauer et al*., 2002b]. The precise source (or sources)

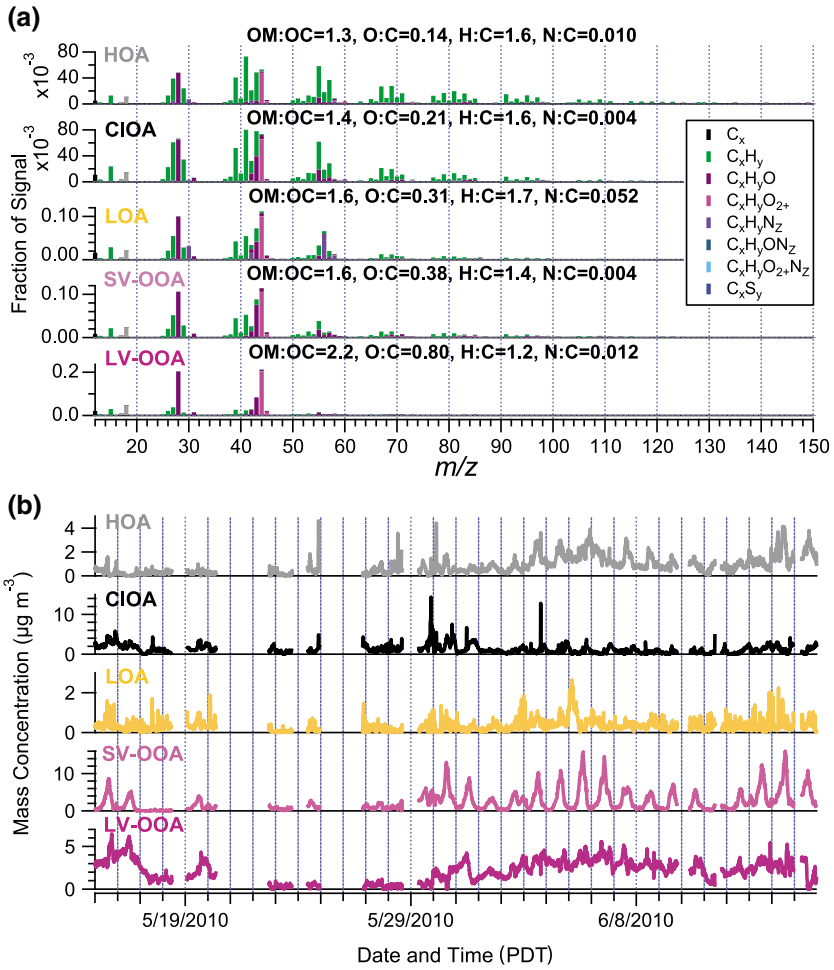

Figure 4. (a) Mass spectra for the five components identified in the PMF analysis. The mass spectra are colored by the ion type to indicate the contribution of each ion type to the mass spectra. For clarity, spectra are shown only to *m/z* 150, although spectra were measured up to *m/z* 204. (b) Time series of the PMF components.

of the LOA component is not known; however, similar, highly variable, nitrogen-rich components have been identified in Mexico City [*Aiken et al.*, 2009]; Riverside, CA [*Docherty et al.*, 2011]; Crete [*Hildebrandt et al.*, 2011]; and New York City [*Sun et al.*, 2011]. This component is termed "local organic aerosol" because the LOA time series exhibits high-frequency fluctuations that indicate a relatively local source for this component. (Autocorrelation plots of the component time series are shown in Figure D-7 of the supporting information.) The LOA mass represents only a small portion of the total OA mass (5%). Still, the reoccurrence of LOA in different urban areas is an interesting finding. Additional details regarding how the PMF solution was selected are provided in section D of the supporting information.

[23] The mass spectra and elemental ratios of the five components displayed in Figure 4a are similar to those reported in previous studies [e.g., *Aiken et al.*, 2009; *Hersey et al.*, 2011; *Mohr et al.*, 2011]. For HOA, O : C is relatively high (0.14) but not out of the range of previously reported values. For instance, O : C values as low as 0.02 (Riverside, CA) and 0.03 (Barcelona) [*Docherty et al.*, 2011; *Mohr et al.*, 2011] and as high as 0.16 (Mexico City) and 0.17 (Beijing) have been reported for HOA components [*Aiken et al.*, 2009; *Huang et al.*, 2010]. The diurnal cycle of HOA is similar to that of EC (and rBC) with a peak between 13:00 and 14:00 PDT (local time), and HOA and EC (and rBC) show high correlation (see Table D-1 in the supporting information and section 3.3 below). Therefore, as discussed in section 3.1, for other primary emissions, it appears that a large portion of the HOA is transported to Pasadena over a period of several hours from the west and south, which is consistent with the relatively high HOA oxidation. Evidence that HOA is dominated by primary sources is given in section 3.4.1. In addition, the Van Krevelen diagram analysis described in the next section indicates that the types of oxygen-containing functional groups in HOA are different from OOA (on average), which suggests a different oxidation pathway(s). A possible cause for the oxygen content in HOA is therefore heterogeneous oxidation, although other causes including primary emission of oxygenates cannot be conclusively ruled out using the results reported here. The CIOA component is more oxygenated than HOA, which is consistent with previous reports and the known presence of oxygenated compounds such as fatty acids and cholesterol in food cooking aerosol [*Mohr et al.*, 2011; *Robinson et al.*, 2006; *Sun et al.*, 2011]. The HOA and CIOA spectra are compared in detail in section D of the supporting

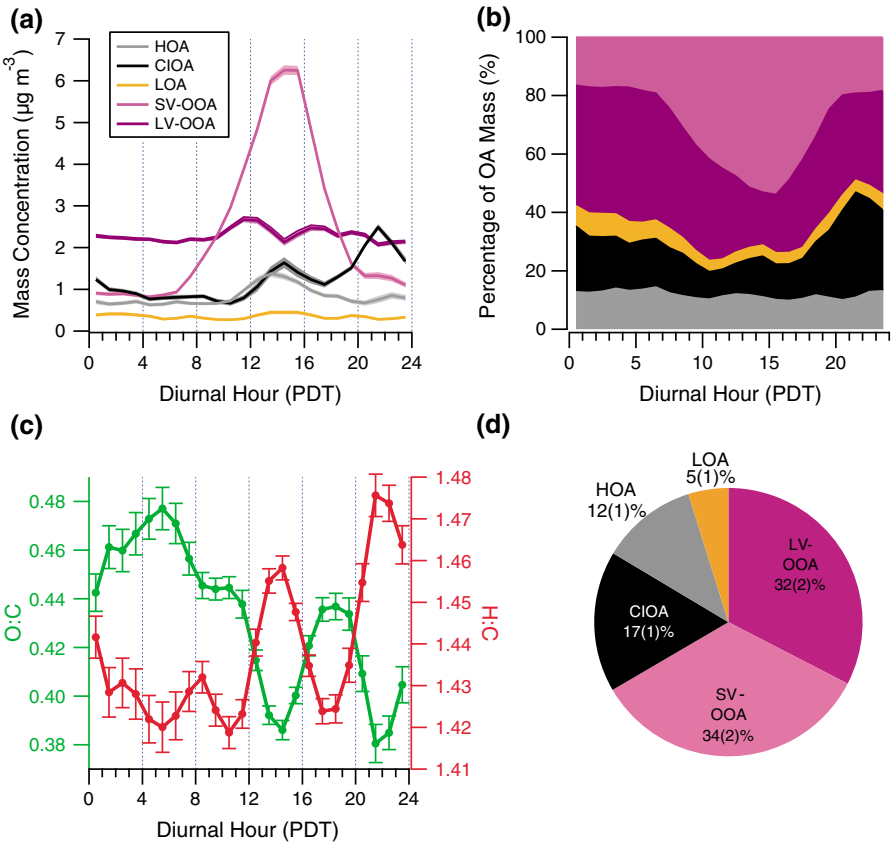

Figure 5. (a) Diurnal profiles for the PMF components. Shaded regions indicate uncertainties calculated using bootstrapping [*Ulbrich et al*., 2009]. (b) Diurnal profiles of the PMF components by percent mass. (c) Diurnal profiles of the oxygen-to-carbon and hydrogen-to-carbon elemental ratios for the total OA mass. Error bars indicate the standard error of the mean. (d) The campaign average contribution of each PMF component to the PM_1 organic aerosol mass concentration.

information. The diurnal cycle of CIOA exhibits peaks near mealtimes with a smaller peak between 14:00 and 15:00 PDT and a larger peak between 21:00 and 22:00 PDT similar to the cooking organic aerosol diurnal cycles observed for other field measurements [*Allan et al*., 2010; *Crippa et al*., 2013; *Mohr et al*., 2011; *Sun et al*., 2011]. The lunchtime and dinnertime peaks are both slightly delayed from traditional American mealtimes. The delays could be due to transport time from areas south and west of Pasadena. The delay in the dinnertime peak may also be the result of the convolution of the emission rates with the lower boundary layer in the evenings and thus reduced vertical dilution of CIOA.

[24] Both SV-OOA and LV-OOA display higher O : C compared to the other OA components for Pasadena, and LV-OOA is the most oxygenated as expected for more aged SOA. The SV-OOA and LV-OOA O : C values (0.38 and 0.8, respectively) are similar to those measured at Barcelona (0.32 and 0.75), New York City (0.38 and 0.68), and Riverside (0.29 and 0.72) [*Docherty et al*., 2011; *Mohr et al*., 2011; *Sun et al*., 2011], and are consistent with the range of O : C values for OOA reported by *Ng et al*. [2011]. The diurnal cycle of SV-OOA is very strong and peaks in the afternoon. This pattern is likely due to photochemical age peaking at a similar time compared to when SOA precursors emitted during the morning rush hour arrive in Pasadena (along with EC and CO). The temporal variability of SV-OOA therefore indicates this component is closely linked to in-basin photochemical production of SOA, as has been seen in other studies [*Aiken et al*., 2009]. In contrast, LV-OOA does not show a strong diurnal variation on average, but the LV-OOA time series does vary substantially during the campaign measurement period. In particular, there is an increasing trend in LV-OOA concentrations during the 2–6 June period when there is evidence for recirculation of polluted air within the South Coast Air Basin impacting aerosol concentrations. A buildup of LV-OOA concentrations during this period is consistent with describing this component as "aged," since the OA is expected to be increasingly oxidized during periods of recirculation.

[25] The mass spectrum of LOA is distinct from the other OA components and contains prominent ions that are characteristic of amines: CH_4N^+ (*m/z* 30), $C_2H_4N^+$ (*m/z* 42), $C_3H_6N^+$ (*m/z* 56), $C_3H_8N^+$ (*m/z* 58), $C_5H_{10}N^+$ (*m/z* 84), and $C_5H_{12}N^+$ (*m/z* 86) [*McLafferty and Turecek*, 1993]. The large contribution of nitrogen to this factor (N : C = 0.05) is explained by the substantial presence of these ions. The contribution of LOA to the total mass for each listed amine fragment ranges from 4% for CH_4N^+ to 89% for $C_5H_{12}N^+$. In total, the LOA component accounts for 34% of the measured amine mass, and the contributions from the other PMF components are 31% (LV-OOA), 15% (HOA), 13% (SV-OOA), and 8% (CIOA). As discussed in section D of

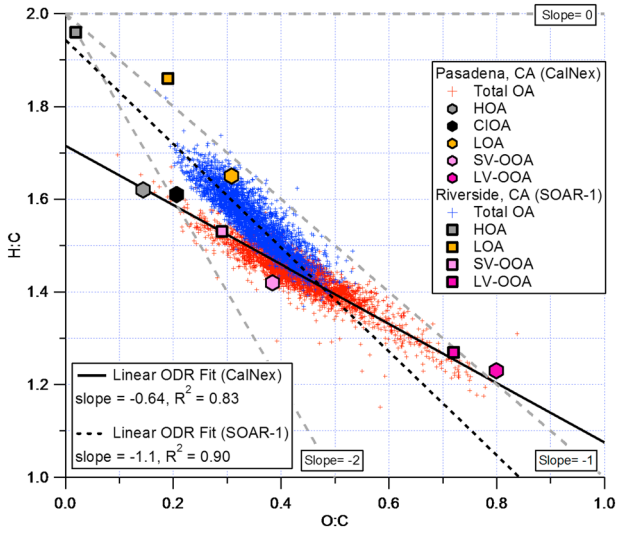

Figure 6. Van Krevelen diagram for Pasadena during the CalNex campaign (red crosses) and for Riverside, CA during the SOAR-1 campaign (blue crosses). The PMF factors identified for Pasadena (hexagons) and Riverside (squares) are shown as well. The linear regression analyses correspond to the total OA data.

the supporting information, the correlations of LOA with other measured species (e.g., VOCs and metals) suggest that LOA sources are related to industrial processes, especially paint application, but the results are not conclusive.

[26] Shown in Figure 5c are the diurnal profiles for the total OA elemental ratios (O : C and H : C). The diurnal trend in the elemental ratios is mostly consistent with the trends in the OA components determined from the PMF analysis. In the early morning hours, the O : C ratio is the highest, which suggests the presence of highly aged, likely secondary, aerosol. Indeed, during this period, LV-OOA is the dominant OA component. In the afternoon (~14:00), there is a strong decrease in O : C, which can be attributed to the arrival of POA at the Pasadena ground site and/or the formation of fresh secondary organic aerosol. In the evening (~21:30), there is second minimum in the O : C, but this occurs during a period of low photochemical age (Figure 2), which implies that the ground site is impacted at this time by POA. As seen in Figure 5, this evening O : C minimum matches the peak in CIOA, a primary OA component with relatively low oxygen content. An interesting difference between the PMF and elemental ratio diurnal trends is the peak in H : C that is observed in the morning (~08:00) and is likely due to primary emissions from the local morning rush hour. This peak is 3 to 4 times smaller than the H : C peaks for the afternoon and evening events also associated with POA, however, indicating a very weak influence from the local rush hour. The PMF analysis is not expected to resolve components that are less than approximately 5% of the OA mass [*Ulbrich et al.*, 2009], and therefore, the absence of this weak local contribution in the PMF results is not surprising.

[27] From Figure 5d, if total OOA is taken as a surrogate for SOA, and the sum of HOA, CIOA, and LOA is taken as a surrogate for POA, then it can be concluded that SOA is dominant at the Pasadena ground site, which is consistent with earlier findings in Riverside, CA [*Docherty et al.*, 2008]. On average, the total OA mass for the measurement period is composed of 66% OOA (SV-OOA + LV-OOA), and this percentage lies between that observed for a selection of "urban" and "urban downwind" sites [*Zhang et al.*, 2007b]. This percentage is also similar to previous results from measurements based in Pasadena. In particular, *Hersey et al.* [2011] reported that during the PACO campaign in May/June 2009, 77% of OA was classified as OOA, and *Turpin et al.* [1991] reported that during the summer of 1984, SOA contributed roughly half of the OA mass. In contrast, there is a wide range of SOA to OA ratios reported for areas east of Pasadena over the past several decades (~20–70%) [*Docherty et al.*, 2008, and references therein].

3.2.2. The Atmospheric Evolution of H : C Versus O : C and the Elemental Ratios of the Organic Aerosol Components

[28] To relate the elemental composition of the OA components to each other as well as to the bulk OA, the H : C and O : C values from the combined AMS/PMF analysis are plotted in a Van Krevelen diagram (Figure 6). Within a Van Krevelen diagram, more oxidized organic compounds lie at the lower right, and different oxidation reactions fall along individual straight lines. For instance, oxidation of a methylene group ($–CH_2–$) to a carbonyl group (–C(=O)–) corresponds to a slope of −2, and oxidation of a methylene group to an alcohol group (–C(–OH)–) corresponds to a slope of 0. Other reactions or combinations of reactions relevant to OA may lead to a variety of slopes in the Van Krevelen diagram as well, which makes attributing a particular slope to a specific chemical reaction difficult in the case of ambient field measurements. Despite this complexity, the Van Krevelen diagram is still useful for constraining the reactions that are responsible for the aging of OA, including for SOA models and their comparison to measurements [e.g., *Murphy et al.*, 2011].

[29] Elemental ratios have been reported previously for the SOAR-1 campaign in Riverside, CA [*Heald et al.*, 2010], and these data are included in Figure 6 as well. The slope of the Van Krevelen diagram for bulk OA is different when comparing the data from Pasadena and Riverside. The regression analysis for Pasadena results in a best-fit slope of –0.64, whereas a slope of –1.1 is obtained for Riverside. However, when the OOA factors are analyzed alone, they correspond to a line with a slope of –0.55 similar to other field measurements [*Ng et al.*, 2011], which is consistent with methylene fragmentation reactions leading to carboxylic acids.

[30] Given that the composition and chemical evolution of OOA in Pasadena and Riverside are similar within this analysis, the differences in the slopes for bulk OA in the Van Krevelen diagram cannot be explained by changes in SOA oxidation chemistry. The composition of the HOA measured at the two locations is dissimilar, however. The HOA in Riverside exhibits a very low O : C ratio (0.02), while in Pasadena, HOA is more oxidized (O : C = 0.14). Thus, it is proposed that the different slope for Riverside is due to the atmospheric mixing of fresh HOA-rich particles into the air mass above the site. In Riverside, the addition of less oxidized HOA to the air mass results in the steep slope observed in that location. Contrastingly, in Pasadena the more oxidized HOA does not influence the slope strongly when mixing occurs because the Pasadena HOA falls near the line defined by the OOA components in the Van Krevelen diagram.

[31] Based on the diurnal cycles of HOA for the two sites, it seems that that the Pasadena HOA is more oxidized because it has undergone more photochemical aging relative to the Riverside HOA. In Riverside, the HOA concentration peaks in the morning as expected for fresh emissions from the local morning rush hour traffic [*Docherty et al*., 2011], consistent with the location of the Riverside site downwind and nearby large highways. In Pasadena, the HOA concentration peaks around 13:30, however, due to advection over several hours from the west and south. We note that the major combustion tracers follow similar diurnal trends for the two sites.

[32] It was also observed by *Ng et al*. [2011] that HOA components occupy a different space of the Van Krevelen diagram relative to OOA and display variability that can be approximated by a line with a −2 slope. The HOA components for Riverside and Pasadena shown in the Van Krevelen diagram presented here follow a similar line, which is indicative of HOA aging. As described already, a slope of −2 is consistent with functionalization of a methylene chain with carbonyls. For Pasadena, the HOA component also correlated with several ketones (see 2DTAG data discussed in section D of the supporting information), which provides further evidence that carbonyl groups may be an important oxygen-containing functional group for HOA.

3.2.3. Constraints on the Biomass Burning Contribution to the Organic Aerosol Mass

[33] An apparent discrepancy between the combined AMS/PMF analysis and the PALMS measurements is that the latter classified 12% of the PM_1 aerosol volume as biomass burning but the AMS does not show a significant amount of biomass burning influence as indicated by the ratio of the organic mass at *m*/*z* 60 to total organic mass (f_{60}) [*Cubison et al*., 2011]. (Note: The possible contribution of organic acids to f_{60} is accounted for by simultaneously analyzing f_{44} in an f_{44} versus f_{60} plot as described previously by Cubison et al.) Also, a biomass burning organic aerosol component is not identified in the PMF analysis, in which OA components accounting for about 5% or more of the OA mass are expected to be resolved [*Ulbrich et al*., 2009]. Acetonitrile, a tracer for biomass burning, is generally near background concentrations (100–150 parts per trillion by volume, pptv) except for several high concentration events that are short in duration, do not correlate with the PALMS biomass burning particles, and could be related to nearby solvent use (e.g., in the Caltech campus). It is possible that potassium-containing particles from sources other than biomass burning such as meat cooking [*Hildemann et al*., 1991; *Schauer et al*., 1999], which can represent a substantial fraction of the potassium in some urban regions [*Aiken et al*., 2010; *Zhang et al*., 2010], may be classified as biomass burning by the PALMS algorithm due to the presence of potassium and abundant organic species. If cooking activities were the dominant source of the PALMS biomass burning particles, however, then the PALMS biomass burning volume concentration would be expected to correlate with the CIOA mass concentration, which is not the case ($R = -0.03$). An alternative explanation is that the primary biomass burning mass is small, and there is a large amount of secondary mass that has condensed on the biomass burning particles. (Similarly, the primary biomass burning particles may have coagulated with secondary aerosol particles.) The particles would then be classified as biomass burning by the PALMS algorithm, but their measured volume would be significantly increased by secondary material (e.g., SOA, nitrate, sulfate, and ammonium). Finally, it is also possible that the biomass burning particles are very aged as the result of long-range transport and that due to aging, they are difficult to identify with the AMS biomass burning tracers or PMF [*Cubison et al*., 2011]. When the observations described in this paragraph are evaluated together, then the best explanation for the discrepancy is that while 12% of submicron particles (by volume) contained some biomass burning material, the overall mass of these particles at the Pasadena ground site was dominated by condensation or particle coagulation of nonbiomass burning material. Based on the limit of AMS/PMF analysis to resolve small fractions of OA, we estimate that primary biomass burning material contributed <5% to submicron aerosol mass during the study.

3.3. Evaluation of Primary Organic Aerosol Emission Ratios With EC and CO

[34] The HOA concentration correlates strongly with EC determined from the online Sunset analyzer ($R = 0.71$), and the ratio of HOA to EC can provide valuable insight regarding the source of this OA component. To explore this correlation further, a scatter plot of HOA versus EC mass concentration data is plotted in Figure 7a. The data points in the plot are colored with the corresponding NO_y to ΔCO ratios. Periods with higher diesel influence are expected to exhibit higher (NO_y/ΔCO) [*Ban-Weiss et al*., 2008a; *Parrish et al*., 2007]. The ratio is not corrected for dry deposition losses of nitric acid though, and thus, it cannot be treated as a quantitative metric. In addition, the gray-shaded areas in Figure 7a indicate the range of POA to EC emission ratios for gasoline and diesel vehicles that were measured during summer 2006 at the Caldecott Tunnel in California [*Ban-Weiss et al*., 2008b]. The HOA to EC ratios at the Pasadena ground site overlap the range of POA to EC ratios from the Caldecott Tunnel. A linear regression analysis of the Pasadena data yields a line with a slope of 1.82, which is close to the upper limit of the POA to EC ratios reported in the tunnel study. The Pasadena ratio is at times higher, but this difference could be due to changes in the emission ratios of vehicles between 2006 and 2010, or the larger influence of cold starts for our data set versus warm-running vehicles for the Caldecott Tunnel. In Pasadena, for periods more influenced by diesel emissions, as indicated by high (NO_y/ΔCO), generally lower HOA to EC ratios are observed. Specifically, the best-fit slope is 1.51 for (NO_y/ΔCO) > 0.124, which corresponds to the highest 10th percentile of (NO_y/ΔCO) values. This finding is consistent with the emission ratios reported by *Ban-Weiss et al*. [2008b] and suggests that both diesel and gasoline vehicle emissions are contributing to the HOA mass.

[35] A correlation between HOA and CO is also observed ($R = 0.59$). A stronger correlation is observed between CO and the sum of HOA and CIOA ($R = 0.71$), however. Shown in Figure 7b is a scatter plot of the CO and the HOA + CIOA data. The improved correlation when the CIOA mass concentration is added to the HOA mass concentration is surprising because cooking is not considered a major source of carbon monoxide, although it is a significant source of organic aerosol [*Allan et al*., 2010; California Air Resources Board, California

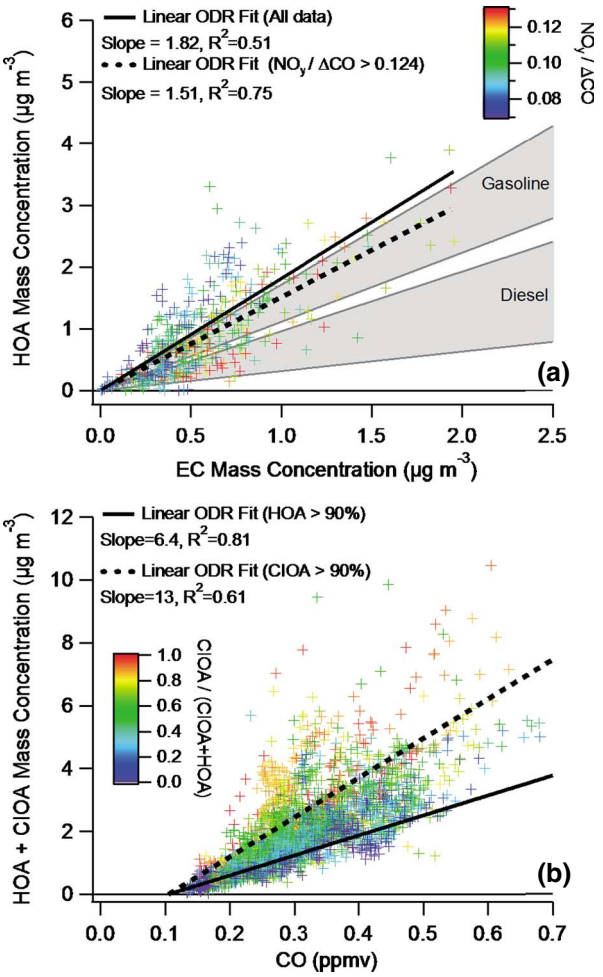

Figure 7. (a) HOA versus EC concentration measured in situ by the Sunset analyzer. Fits are shown for the entire plot (solid line) and for only data points corresponding to high $NO_y/\Delta CO$ ratios (dashed line). The gray-shaded regions indicate the range of expected slopes for gasoline and diesel vehicles based on the reported emission ratios of *Ban-Weiss et al.* [2008b] and a 1.34 OM : OC. (b) The sum of HOA and CIOA versus CO concentration. Linear fits are shown for data points corresponding to high HOA (solid line) and high CIOA concentrations (dashed line).

emission inventory data, 2008, http://www.arb.ca.gov/ei/emsmain/emsmain.htm; *Harley et al.*, 1997]. Emissions of CO have been measured from certain cooking activities [*Lee et al.*, 2001], but it is still a possibility that the CIOA component contains particulate mass from noncooking sources that also emit CO (e.g., gasoline vehicles). Therefore, it is most reasonable to characterize this component as "cooking-influenced" but not purely from cooking sources. It should be noted that different PMF solution rotations were explored using the FPeak parameter as discussed in the supporting information. There are rotations that exhibit lower correlations between CIOA and CO, but HOA + CIOA always displays a higher correlation than HOA with CO (within the constraint of not substantially diminishing the correlation between HOA and rBC). In addition, these alternative solutions exhibit lower correlations between HOA and rBC, as well as between HOA + CIOA and CO.

[36] The data in Figure 7b are also colored by the relative amount of CIOA, so that the ratios of HOA to CO and CIOA to CO can be at least partially resolved. For periods when HOA concentrations are high (i.e., greater than 90% of the sum of HOA and CIOA), the correlation with CO is very strong (R = 0.9) and the linear slope is 6.4 $\mu g\,m^{-3}$ $ppmv^{-1}$ when using a CO background (*x* intercept) of 105 ppbv, which is comparable to slopes found in previous studies [*Aiken et al.*, 2009]. In contrast, for periods when CIOA concentrations are high, the linear slope is 13 $\mu g\,m^{-3}$ $ppmv^{-1}$, more than twice that for HOA. The steeper slope for CIOA is indicative of significant cooking sources for CIOA that, as stated earlier, produce a larger amount of organic aerosol relative to CO [*McDonald et al.*, 2003]. A lower limit on the relative amount of CIOA mass from cooking sources can be estimated using the observation that the linear regression slope of CIOA is about twice that of HOA when the mass concentrations are plotted versus CO. Assuming that CO is overwhelmingly from vehicle emissions and no CO is emitted from cooking sources, then CIOA would be 50% from cooking sources *on average* with the remainder from vehicle emissions (i.e., the additional cooking organic aerosol mass would double the mass concentration versus CO slope relative to HOA). This percentage is a lower limit because some CO could be coemitted with cooking organic aerosol, for instance, from burning of charcoal [*Bhattacharya et al.*, 2002], and that would raise the percentage of CIOA from cooking above 50%. This approach is a simplistic approximation, but the lower limit appears to be reasonable given that the diurnal cycles and spectral characteristics of CIOA are consistent with previous studies. In addition, comparison of the CIOA concentration against that predicted from the amount of organic mass measured by the AMS at *m/z* 55 following *Mohr et al.* [2011] indicates that approximately 75% of CIOA is from cooking sources (see section D of the supporting information for the details of this comparison). A higher percentage up to almost 100% is also possible given the uncertainties in the comparison.

[37] An alternative approach for analyzing the correlation with CO is to use a multilinear regression instead of filtering the data for periods of high HOA or CIOA influence. For completeness, a multilinear regression was performed where HOA and CIOA were the independent variables and CO was the dependent variable. Emission ratios of 8.0 and 16 $\mu g\,m^{-3}$ $ppmv^{-1}$ were obtained for HOA and CIOA, respectively (using 105 ppbv background CO as above). This result is similar to that described in the preceding paragraph, which indicates both approaches for treating the data are robust.

3.4. The Quantitative Dependence of Secondary Organic Aerosol Concentration on Photochemical Oxidation

3.4.1. Increases in the Organic Aerosol to ΔCO Ratio With Photochemical Age

[38] To evaluate if the timescales and efficiency of SOA formation observed in Pasadena are similar to other urban regions the evolution of (OA/ΔCO) as a function of photochemical age is plotted in Figure 8, where ΔCO is the CO concentration enhancement over its background concentration. The background CO is estimated to be between 85 and 125 ppbv using CO measurements taken aboard the NOAA WP-3D aircraft off the LA coastline at altitudes less

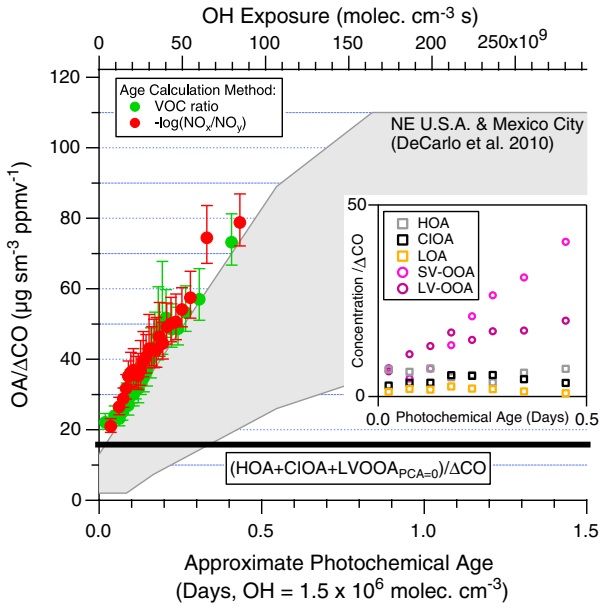

Figure 8. The evolution of OA/ΔCO versus photochemical age for Pasadena during CalNex. The measured ratios are averaged into 25 bins according to photochemical age. The enhanced CO (ΔCO) is the ambient CO minus the estimated background CO (105 ppb). The standard error of OA/ΔCO is smaller than the size of the data point and therefore is not plotted. Instead, error bars representing the uncertainty in the ratio due to an uncertainty of ±20 ppbv in background CO are shown. Photochemical age is determined by two methods: (1) following *Parrish et al*. [2007] and using the ratio of 1,2,4-trimethylbenzene to benzene (green), and (2) following *Kleinman et al*. [2008] and defining the photochemical age as $-\log_{10}(NO_x/NO_y)$ (red). All photochemical ages have been standardized to an OH radical concentration of 1.5×10^6 mol cm^{-3}, and the corresponding OH exposure for a given photochemical age is shown on the top axis. The gray region is adapted from *DeCarlo et al*. [2010] and represents the evolution of OA/ΔCO observed in the northeastern United States and the Mexico City area. The black horizontal line is the ratio of (HOA + ClOA + "background LVOOA") to ΔCO. (Inset) Evolution of the PMF component concentrations normalized to ΔCO versus photochemical age. Data are binned according to photochemical age.

than 200 m (Latitude range: 32 to 35, Longitude range: −117 to −120). A concentration of 102 ppbv was the minimum observed and concentrations below 110 ppbv were regularly observed. Accordingly, the background CO was taken to be 105 ppb when calculating (OA/ΔCO), and the error bars in Figure 8 represent the variability in the data if the background CO is taken to be either 85 or 125 ppb. Given the observed CO values off the LA coastline this range represents a conservative estimate of the uncertainty in background CO. The CO enhancement is assumed to be a conservative tracer of urban combustion emissions that are also a source of aerosols and aerosol precursors, and thus, normalizing the OA concentration to CO will remove the effect of dilution. Photochemical formation of CO from VOCs or destruction of CO by OH reactions were estimated to perturb CO concentrations minimally over these time and spatial scales [*Griffin et al*., 2007].

[39] The gray region in Figure 8 represents OA/ΔCO versus photochemical age observations from previous campaigns in Mexico City and the northeastern United States as summarized by *DeCarlo et al*. [2010]. All the data sets display an increase in the OA/ΔCO ratios with photochemical age due to secondary organic aerosol formation. The Pasadena OA/ΔCO versus photochemical age plot follows the upper limit of the range of previously reported values, although the differences should not be over interpreted given the uncertainties associated with the background CO determination (indicated by the error bars) and the photochemical age calculations. The photochemical age uncertainty has been discussed extensively in previous papers and is due to, in part, the presence of mixed sources with different emission profiles and spatial distributions [e.g., *Kleinman et al*., 2007; *Parrish et al*., 2007]. We evaluate this potential source of error in section E of the supporting information, and use sensitivity studies to determine that photochemical age may be underestimated by approximately 10% in our analysis. This error is in the accuracy rather than the precision, and thus, it does not impact relative comparisons for Pasadena such as the weekday versus Sunday comparison described below. The underestimation may impact comparisons with other campaigns though, and thus it is concluded that SOA production per unit CO in the South Coast Air Basin is not different from other locations given our estimated errors. (In section E of the supporting information, we also demonstrate that OH radical chemistry dominates over Cl radical chemistry in the oxidation of the VOCs used to calculate photochemical age.) The data in Figure 8 suggest that similar precursors are responsible for SOA production in Pasadena, Mexico City, and the northeastern United States, and that the precursors are emitted proportionally to CO. These conditions then imply a relatively constant mix of the important SOA precursor and CO sources across the locations discussed.

[40] To understand the similarity in OA/ΔCO, it is important to consider the emission ratios for SOA precursors (e.g., ΔVOC/ΔCO), especially given the long-term decrease of CO concentrations in the United States [*Parrish et al*., 2002] that could potentially influence OA/ΔCO values. The emission ratios of aromatic, alkyne, and alkene VOCs with CO have remained constant between 2002 and 2010, as has the ratio for acetaldehyde [*Warneke et al*., 2012], a species that correlates strongly with OOA (R = 0.81 in Pasadena) and is dominated by secondary sources after sufficient photochemical processing of emissions. Furthermore, it has been shown that urban VOC emissions at different locations in the U.S. have similar composition and emission ratios with CO (within a factor of 2) [*de Gouw et al*., 2012; *Warneke et al*., 2007]. The similarity of OA/ΔCO values described here for different campaigns spanning several years is consistent with the lack of change in ΔVOC/ΔCO over spatial and temporal scales for the U.S. However, in Mexico City, the ΔVOC/ΔCO ratios are on average about a factor of 2 higher than that in the U.S. [*Bon et al*., 2011], but the OA/ΔCO values for Mexico City are not substantially higher than that for Pasadena or the northeastern U.S. This observation highlights the possibility that there may be unmeasured organic compounds that are SOA precursors and do not follow the ΔVOC/ΔCO emission trends discussed above. Lastly, we note that while plotting OA/ΔCO versus photochemical age should account for differences in the amount of aging, the

average daily OH radical concentrations at the sites were fairly similar where measurements were available: 1.3×10^6 mol cm^{-3} for Pasadena and 1.5×10^6 mol cm^{-3} for Mexico City [*Hodzic and Jimenez*, 2011].

[41] Marked in Figure 8 is the sum of HOA, CIOA, and background LV-OOA ($LVOOA_{PCA=0}$) divided by CO. The ratio of HOA + CIOA to CO is determined from the linear regression analysis of the data in Figure 7b, and the background LV-OOA to CO ratio is the average of LV-OOA divided by CO at photochemical ages less than 0.05 days (Figure 8 inset). Several explanations are possible for the source of background LV-OOA. First, some very aged SOA may be present due to recirculation in the LA basin, for which the photochemical tracers have mostly decayed away. However, the similarity in calculated photochemical ages using either (trimethylbenzene/benzene) or (NO_x/NO_y) suggests that this scenario is not the case, since the high deposition velocity of nitric acid would lead to an observed discrepancy between the two methods at high photochemical ages. A second plausible explanation is "dark" SOA production from ozone or nitrate radicals that will react with alkenes and PAHs. An important piece of evidence to support this possibility would be an increase in OA/ΔCO at low photochemical ages as the time of day approached sunrise, since the increase in morning traffic would lead to fresh emissions that decrease photochemical age and react with ozone or nitrate radical to form SOA. This phenomenon is not observed, however, which indicates that "dark" SOA is not an important source of the background LV-OOA, consistent with the expected minor contribution of alkenes to SOA in urban areas [*Dzepina et al*., 2009; *Wood et al*., 2010].

[42] A third explanation is that marine OA may be contributing to the background LV-OOA. However, the very low OA concentrations, less than 0.2 μg m^{-3}, over the open ocean west of California for periods with low pollution influence (P. K. Quinn, NOAA, personal communication, 2012) indicate that this source is less important. In addition, low marine OA concentrations, 0.5 μg m^{-3}, have been measured by an AMS in La Jolla, CA (located on the California coast 170 km southeast of Pasadena) [*Liu et al*., 2011], which is an amount similar to other marine studies [*Russell et al*., 2010], and would only account for a third of the background LV-OOA.

[43] The last and most likely explanation for the background LV-OOA is the influence of biogenic sources that emit SOA precursors but relatively small amounts of 1,2,4-trimethylbenzene, benzene, NO_x, and CO [*Slowik et al*., 2010]. If the air mass above Pasadena was influenced by a biogenic source, an increase in OA/ΔCO would be observed, but the photochemical age as measured by the ratio of (1,2,4-trimethylbenzne/benzene) or (NO_x/NO_y) would not be significantly altered. Back trajectories for air reaching Pasadena during CalNex often travel over the coastal California mountain ranges where biogenic VOC emissions are large (see section A of the supporting information). Interestingly, at low photochemical ages (less than 0.05 days), there is a general increase in OA/ΔCO with the sum of the concentrations of the two isoprene oxidation products measured by the GC-MS. In particular, when averaging the data into the three bins corresponding to low, medium, and high concentrations of MVK plus methacrolein, the binned OA/ΔCO increases from 21 to 26 μg sm^{-3} ppmv^{-1} (standard errors are less than 0.5) from the lowest third to the highest third. This observation indicates that biogenic sources are influencing OA/ΔCO. Furthermore, ^{14}C measurements for selected days during CalNex show that in the early morning hours when LV-OOA is dominant (compared to other OA components and EC), about 50% of total carbon is nonfossil (e.g., from modern sources) [*Bahreini et al*., 2012]. These results are consistent with biogenic sources influencing the OA/ΔCO ratio and substantially contributing to background LV-OOA (P. Zotter et al., manuscript in preparation, 2012).

[44] In the Figure 8 inset, the organic mass to ΔCO ratio is plotted for each PMF component. The ratio increases for SV-OOA and LV-OOA with photochemical age consistent with both components being dominated by secondary sources. In contrast, the ratios for HOA, CIOA, and LOA do not vary substantially with photochemical age, which strongly supports that these three components are dominated by primary sources. The data in Figure 8 also allow for estimating the amount of background OA (i.e., OA from long range transport). As described above, the concentration of LV-OOA at the lowest photochemical ages should approximately correspond to background OA. Taking LV-OOA/ΔCO for the lowest age bin in Figure 8 and multiplying it by the ΔCO for this bin yields a background OA concentration of 1.5 μg m^{-3}.

[45] For HOA, heterogeneous oxidation could potentially increase or decrease the magnitude of HOA/ΔCO through either functionalization or fragmentation reactions, respectively. Given the Van Krevelen diagram analysis described above in section 3.2.2, fragmentations reactions appear not to be the dominant oxidation pathway. This conclusion is consistent with the recent work of *Lambe et al*. [2012] that showed that for larger alkanes, the onset of fragmentation occurs at an O : C of about 0.3, which is much higher than the O : C of HOA reported here (0.14). For functionalization reactions, based on the OM : OC ratio of 1.3 for HOA and an estimated OM : OC of 1.2 for an un-oxidized alkane chain, it is calculated that the increase in HOA mass due to oxidation is only 8%, which is smaller than the standard deviation (21%) of the data shown in Figure 8. Condensation of primary semivolatile organic compounds could also potentially increase HOA/ΔCO since the averaged OA mass concentration increases with photochemical age from 5 to 15 μg m^{-3} for the binned data shown in Figure 8. However, an increase in HOA/ΔCO with photochemical age is not observed in Figure 8. This result is consistent with the calculated change in HOA concentrations due to partitioning. Specifically, using the volatility distribution for POA and primary semivolatile organic compounds reported by *Robinson et al*. [2007], it is calculated that the increase in HOA concentrations (and HOA/ΔCO) would be only 28% for an increase of OA from 5 to 15 μg m^{-3}. This calculated increase is similar in magnitude to the standard deviation of HOA/ΔCO and, hence, would be hard to discern. In addition, it is substantially smaller than the increase observed for SV-OOA/ΔCO (540%) and LV-OOA/ΔCO (300%). The considerations described in this paragraph also apply to CIOA and LOA but are more difficult to quantify for these components given the lack of literature data (e.g., fragmentation reaction studies and volatility distributions).

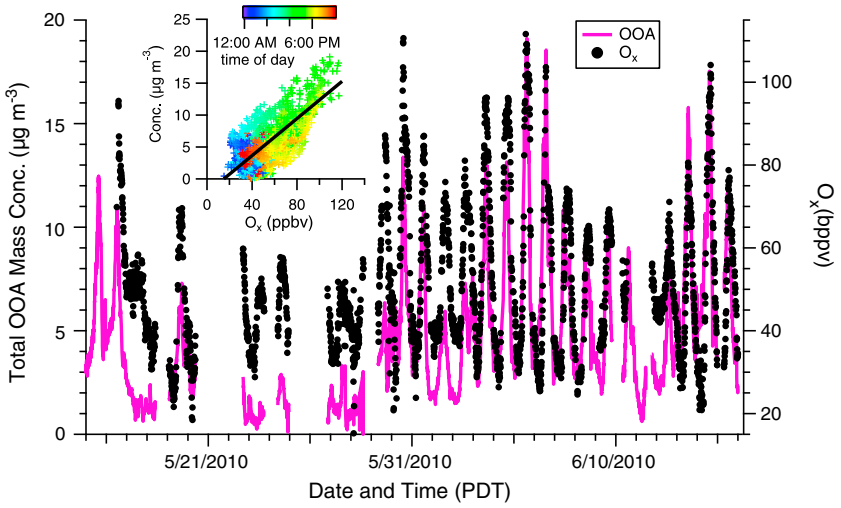

Figure 9. Time series for OOA (the sum of SV-OOA and LV-OOA) and O_x (the sum of O_3 and NO_2). (Inset) Scatter plot of OOA versus O_x with linear fit and colored by time of day. The best-fit slope is 0.146 ($R^2 = 0.53$). A fixed *x* intercept of 15 ppmv O_x is used in the fitting procedure identical to previously published work.

3.4.2. Correlation of Oxygenated Organic Aerosols With the Photochemical Oxidation Marker Odd-Oxygen ($O_3 + NO_2$)

[46] Odd-oxygen, O_x, concentrations are closely linked to the extent of photochemical oxidation in an air mass because O_3 production results from OH reactions with VOCs and CO. Therefore, the ratios of OOA to odd-oxygen provide another metric for quantifying the dependence of SOA concentration on photochemical oxidation. Following the work of *Herndon et al*. [2008] and *Wood et al*. [2010], we examine the correlations of O_x instead of O_3 to account for the titration of O_3 by fresh NO emissions which produces NO_2. When comparing the time series of total OOA (SV-OOA + LV-OOA) versus O_x in Figure 9, similar temporal changes are observed ($R^2 = 0.53$), but the correlation is stronger during the more polluted periods of high OOA concentrations that occurred in June ($R^2 = 0.72$ for the 2–6 June high pollution period). It has also been observed that for long-range transported air, the correlation vanishes due to differing losses and ongoing chemistry of SOA and O_x [*Dunlea et al*., 2009]. In Pasadena, the regression slope for OOA versus O_x is 0.146(±0.001) μg sm^{-3} $ppbv^{-1}$ (Figure 9 inset). The data in the scatter plot are colored by time of day, and interestingly, the slope observed for the morning (06:00–12:00 PDT) is steeper than the slope in the afternoon (12:00–18:00 PDT): 0.183(±0.004) versus 0.163(±0.002) μg sm^{-3} $ppbv^{-1}$. This trend has also been observed in other field measurements [*Herndon et al*., 2008; *Wood et al*., 2010] and has been attributed to several factors including increased evaporation of SV-OOA, mixing with air aloft that contains residual OOA and O_x during boundary layer growth, and OOA production occurring on shorter timescales than O_x. The slopes of identical analyses for Riverside, CA and Mexico City are 0.142 (±0.004) and 0.156(±0.001) μg sm^{-3} $ppbv^{-1}$ [*Aiken et al*., 2009; *Docherty et al*., 2011], which are similar to the Pasadena ground site. This agreement indicates that the ratios of the SOA to O_x production rates are remarkably constant for the different sites suggesting similar SOA and O_x formation chemistries on average. As discussed by *Wood et al*. [2010], changes in the OOA/O_x ratio would be expected at locations where the relative concentrations of SOA and O_x precursors are different. In Houston, for instance, ratios as low as 0.030 μg sm^{-3} $ppbv^{-1}$ were found in correlation analyses during periods impacted by large petrochemical plant emissions. This observation was explained by very high concentrations of light alkenes that cause high ozone concentrations but are not expected to contribute greatly to SOA formation. Contrastingly, in Riverside, the relative concentrations of SOA and O_x precursors are expected to be similar to Pasadena given that urban VOC emissions have similar composition and emission ratios throughout the U.S. [*Warneke et al*., 2007] and have not changed over the past several years [*Warneke et al*., 2012]. In Mexico City, the emission ratios for VOCs (i.e., VOC/CO) are generally higher by a factor of approximately 2 [*Bon et al*., 2011], which would impact both SOA and O_x production rates proportionally. An important exception is the emission ratios for propane and butane, which were disproportionality high in Mexico City due to liquid petroleum use [*Apel et al*., 2010]. The contribution of these light VOC compounds was found to be small for O_x production and zero for SOA production, however [*Wood et al*., 2010]. Similar to the OA/ΔCO discussion in the preceding section, the consistency in OOA/O_x for multiple field campaigns suggests a relatively constant mix of different O_3 and SOA precursor sources, leading to similar production ratios across multiple urban locations in North America. As also discussed above, the insensitivity of OA/ΔCO to differences in VOC/CO suggests unmeasured precursors, but if these unidentified species were emitted in proportion to other VOCs, then consistent OOA/O_x values would be expected for the different locations.

[47] Chlorine radicals are expected to play a larger role in ozone formation for Pasadena and Riverside in comparison to Mexico City, since the first two locations are near the Pacific Ocean. The contribution of chlorine radical chemistry to the total ozone concentration is a topic of current research [*Young et al*., 2012]. Still, published work [*Knipping and Dabdub*, 2003] indicates that in Pasadena and Riverside, it is relatively small and, as a percentage, less than the 30%

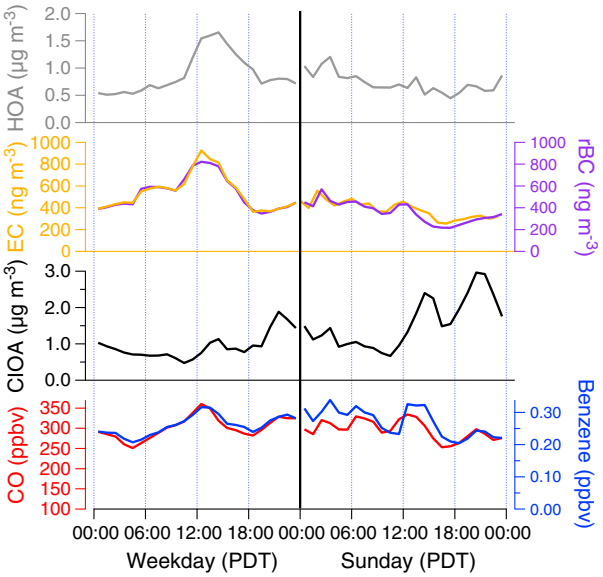

Figure 10. Diurnal profiles, calculated using means, of HOA, EC, rBC, CIOA, CO, and Benzene for weekdays and Sundays during CalNex.

uncertainty for AMS measurements [*Middlebrook et al.*, 2012], which is expected to dominate in the OOA/O_x comparison. Thus, the similarity of OOA/O_x between the three locations is consistent with previous work on chloride radical chemistry in the South Coast Air Basin.

[48] Meteorological parameters could also influence OOA/O_x in a number of ways through changes in OOA partitioning with temperature or increases in the importance of aqueous chemistry at high RH. These parameters do not appear to be important for the OOA/O_x analysis presented here, however. The average temperatures and RHs for the different sites with similar OOA/O_x were as follows: 18 °C and 83% (Pasadena), 27 °C and 53% (Riverside), and 16 °C and 50% (Mexico City). While higher temperatures in Riverside will favor partitioning of OOA to the vapor phase, the measured volatility of OA for Riverside [*Huffman et al.*, 2009] indicates the amount of evaporation will be small (less than 10%) and, thus, will have little effect on OOA/O_x. Additionally, the higher RH in Pasadena relative to Riverside and Mexico City may not influence OOA concentrations given that aerosol water was not an important absorbing phase [*Zhang et al.*, 2012] as discussed in section 3.1.

3.5. Weekly Cycles for Organic Aerosol Components

3.5.1. Weekly Cycles: Primary Organic Aerosols

[49] It is well known that in California and the South Coast Air Basin, a large decrease in on-road diesel vehicle activity occurs on weekends, which leads to significant reductions in atmospheric species associated with diesel vehicles such as NO_x, EC, specific VOCs, and particulate nitrate [*Marr and Harley*, 2002; *Millstein et al.*, 2008; *Pollack et al.*, 2012]. To explore if primary organic aerosols show an analogous weekend effect in Pasadena during CalNex, the diurnal cycles for HOA, EC, rBC, CIOA, CO, and benzene are plotted for weekdays and Sundays separately in Figure 10. Included in the Sunday diurnal cycle is data from the Memorial Day holiday, which occurred on a Monday and exhibited traffic patterns typical of Sundays [*Caltrans*, 2010]. Thus, the "Sunday" diurnal cycle combines data from 6 days. Saturday data are not included in Figure 10 to avoid carryover effects from the preceding Friday. Carryover effects on Mondays appear to have little impact on the weekday diurnal cycle with less than 3% change in the average daily concentrations when Mondays are omitted from averaging and no qualitative change in the diurnal cycles. Thus, Monday data are included with the other weekday data in Figure 10.

[50] The EC (and rBC) concentration decreases on Sundays to 71(±6)% of its weekday average and has a very different diurnal cycle. A similar change is observed for HOA, which decreases to 82(±4)% of its weekday average. (Note: Uncertainties are the standard errors of the mean.) The decrease in concentrations is consistent with the weekend effect and the importance of diesel vehicle emissions as a source for HOA and EC (and rBC). In contrast, CO concentrations when integrated over the entire day are not substantially different on Sundays versus weekdays, and the average concentration on Sundays is 99.4(±0.3)% of the weekday average. The CO diurnal cycles are dissimilar probably due to changes in traffic patterns. Benzene displays a similar lack of change on Sundays increasing to 105(±3)% of the weekday average. Since gasoline vehicles are an important source of CO and benzene [*Fruin et al.*, 2001; *Schauer et al.*, 2002a], the lack of a weekend effect for these compounds is consistent with previous studies that demonstrated similar overall activity for gasoline vehicles on weekends compared to weekdays [*Marr and Harley*, 2002; *Pollack et al.*, 2012]. The CIOA concentrations are elevated on Sundays by 161(±4)% displaying a weekly cycle distinctly different from the other species in Figure 10. An increase in barbecuing on weekends has been reported previously for the South Coast Air Basin [*Chinkin et al.*, 2003], which is consistent with elevated CIOA concentrations on weekends. However, given the limited corroborating evidence and lack of previous long-term observations of cooking emissions (to our knowledge), further studies are needed to make a confident conclusion regarding the weekly variations in cooking organic aerosol.

[51] The observed decreases in HOA and EC concentrations on Sundays can be compared against the expected decreases in their emissions, estimated from a combination of data on fuel sales (California State Board of Equalization, Fuel Taxes Statistics and Reports, 2011, http://www.boe.ca.gov/sptaxprog/spftrpts.htm, hereinafter referred to as California State Board of Equalization, online report, 2011), emission ratios [*Ban-Weiss et al.*, 2008b], and traffic volume [*Caltrans*, 2010]. The first step to obtain the estimates is calculating the percentage of weekday EC and HOA attributable to diesel emissions using equation (1) below.

$$\frac{EC_{\mathrm{Diesel}}}{EC_{\mathrm{Total}}} = \frac{ER_{\mathrm{Diesel}} \times FS_{\mathrm{Diesel}}}{(ER_{\mathrm{Diesel}} \times FS_{\mathrm{Diesel}}) + (ER_{\mathrm{Gasoline}} \times FS_{\mathrm{Gasoline}})} \quad (1)$$

[52] In equation (1), *ER* is the emission ratio for diesel and gasoline vehicles taken from *Ban-Weiss et al.* [2008b], and *FS* is the gasoline and diesel fuel sales reported for the state of California during May and June 2010 (California State Board of Equalization, online report, 2011). An analogous equation is used for HOA. The *ER* is defined as the amount

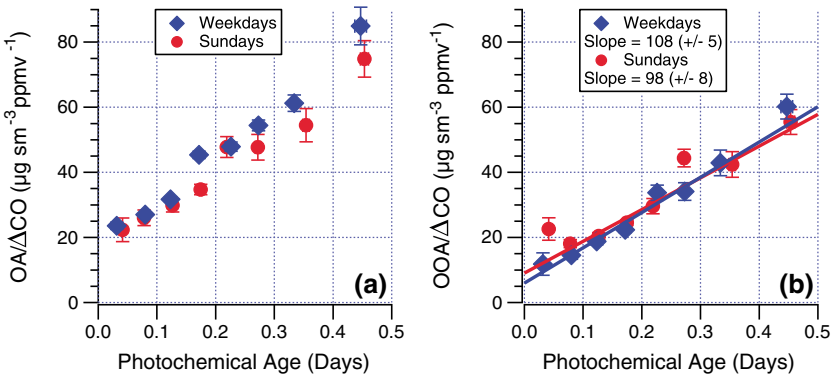

Figure 11. (a) The evolution of OA/ΔCO versus photochemical age for Pasadena during CalNex separated by day of the week. The enhanced CO (ΔCO) is the ambient CO minus the estimated background CO (105 ppb). Error bars indicate the standard errors. Photochemical age is determined using the method of *Parrish et al*. [2007]. (b) Also shown is the analogous plot for OOA with the linear ODR fits of the data.

of EC (or HOA) emitted per unit fuel burned, and the values used in this work are 0.022 (gasoline EC), 0.86 (diesel EC), 0.031 (gasoline HOA), and 0.41 g kg^{-1} (diesel HOA). It is assumed that the monthly fuel sales are representative of weekday fuel use in the South Coast Air Basin. Following this method, it is estimated that diesel emissions account for 87 (±3)% of EC and 70(±10)% of HOA. The second step utilizes daily vehicle miles traveled (VMT) data for Los Angeles County to calculate that during the campaign truck traffic decreased 44% on Sundays relative to weekdays [*Caltrans*, 2010]. This figure lies within the range of other estimates for weekend reductions of heavy-duty vehicle traffic [*Chinkin et al*., 2003]. Finally, an estimate of EC concentrations on Sunday relative to weekdays, ΔEC_{sun} (%), can be calculated as follows (an analogous equation can be used for HOA).

$$\Delta EC_{\mathrm{Sun}} = \frac{EC_{\mathrm{Diesel}}}{EC_{\mathrm{Total}}} \times \frac{(Truck\ VMT)_{\mathrm{Sun}}}{(Truck\ VMT)_{\mathrm{WD}}} + \frac{EC_{\mathrm{Gas}}}{EC_{\mathrm{Total}}} \times \frac{(Non-Truck\ VMT)_{\mathrm{Sun}}}{(Non-Truck\ VMT)_{\mathrm{WD}}} + \frac{EC_{\mathrm{Background}}}{EC_{\mathrm{Total}}} \quad (2)$$

[53] Using equation (2), the Sunday concentrations of EC and HOA are estimated to be 64(±3)% and 72(±6)% of their weekday concentrations, respectively. To estimate these values, the nontruck VMT on Sundays versus weekdays was taken to be equal because of the similarity in the average daily CO and benzene concentrations. In addition, the background EC is the average of the values from *Langridge et al*. [2012], 40(±20) ng m^{-3}, and the background HOA, 70(±40) ng m^{-3}, was calculated from EC using the slope of HOA to EC reported in Figure 7. (Note: The uncertainties for the calculated Sunday reductions in EC and HOA include the uncertainties in the background concentrations reported in Langridge et al.) For comparison, the observed average Sunday EC and HOA concentrations at the Pasadena ground site are 71(±6)% and 82(±4)% of the weekday averages, respectively. The agreement between the estimated and observed values is good, given the need for several approximations to obtain the estimate. The reduction in HOA is less than the reduction in EC for both the estimated and observed values, due to the greater portion of HOA emitted from gasoline vehicles. It is noted that in contrast to HOA, the CIOA concentration is higher on Sundays as discussed above, and the combination of the two opposite trends leads to a net increase of POA on the weekends.

[54] An important assumption of this analysis is that the only sources of EC are on-road diesel and gasoline emissions, as well as the background from long-range transport. Transport is the single largest source of EC in the United States, and in the absence of biomass burning, it accounts for 81% of emitted EC. Within the transport sector, EC emissions are dominated by on-road and non-road diesel (U.S. Environmental Protection Agency, Black carbon: Basic information, 2012, http://www.epa.gov/blackcarbon/basic.html). Another question is whether commercial marine emissions may have a substantial contribution to the EC budget. To address this consideration, we examined the correlation between EC and the oil combustion particles identified by the PALMS instrument, which are presumably from shipping activities. We observed a low correlation ($R^2 = 0.24$), which is consistent with commercial marine EC emissions not substantially impacting the ground site. Ultimately, accounting for only three sources of EC (on-road diesel, on-road gasoline, and a background) is a simplifying assumption, but one that is consistent with emission inventories and other observations. The reasonableness of this assumption is further supported by the closure obtained between the calculated and measured weekly cycles.

3.5.2. Weekly Cycles: Secondary Organic Aerosols and Constraining the Importance of Diesel Emissions

[55] To evaluate the weekly cycle for secondary organic aerosols, OA/ΔCO versus photochemical age is plotted in Figure 11a for weekdays and Sundays. Also shown is the analogous plot for total OOA (Figure 11b). The OOA plot is similar for weekdays versus Sundays, and linear regression analyses of the data yield slopes of 108(±5) and 98(±8) μg sm^{-3} ppmv^{-1} for weekdays and Sundays, respectively. (Note: The data fitted are averages resulting from binning the raw data according to photochemical age, and the averages are weighted by the standard errors of the *x* and *y* data.) After propagation of error, these slopes correspond to a ratio of 1.1(±0.1) for weekdays to weekends. Following the estimation method described by

Bahreini et al. [2012], and using a 44% decrease in diesel traffic on Sundays as determined above, this ratio corresponds to diesel emissions accounting for 19(+17/−21)% of the OOA mass. Also, a consistently higher photochemical age is observed on Sunday versus weekdays due to the higher oxidant concentrations resulting from reduced NO_x emissions. These results are in good agreement with other CalNex papers that address weekday/weekend effects [*Bahreini et al*., 2012; *Pollack et al*., 2012]. In particular, they are consistent with the conclusion reported by *Bahreini et al*. [2012] that gasoline emissions are substantially more important than diesel emissions in the formation of secondary organic aerosol mass within the LA Basin, since a large decrease in the OOA/ΔCO ratio is not observed on weekends when there is less diesel traffic. It should be noted as well that the results present here are better constrained than the Bahreini et al. analysis because the PMF results are used to obtain OOA/ΔCO rather than relying on estimated values of POA/ΔCO to calculate OOA/ΔCO and because of the more precise binning by photochemical age.

[56] We note that for the diesel versus gasoline analysis presented in the preceding paragraph, three important assumptions are made. First, it is assumed that SOA precursors in the South Coast Air Basin are dominated by motor vehicle emissions. While this is consistent with measured VOC/CO ratios [*Warneke et al*., 2012], the possibility of important and unidentified SOA precursors from nonvehicular sources cannot be completely ruled out. Therefore, further research is needed to constrain the contribution of nonvehicular sources to SOA.

[57] The second important assumption is that some of the SOA measured may be due to long-range transport, which is not accounted for in the preceding analysis. To at least partially account for this possible source of error, we repeat the analysis above but only for photochemical ages above 0.1 days. Photochemical ages above 0.1 days generally occur during daytime when the higher amount of SV-OOA versus LV-OOA indicates that SOA production is more local and recent. The resulting slopes of the regression analyses are 121(±7) and 115(±10) $\mu g\ sm^{-3}\ ppmv^{-1}$ for weekdays and Sunday, respectively, and then the ratio of the slopes is 1.0(±0.1). This ratio corresponds to diesel emissions accounting for −2(+21/−26)% of the OOA mass. The upper limit of this range is less than that for the original analysis (36%) for all photochemical ages. Thus, we report the 19(+17/−21)% result, since it is more conservative and represents the entirety of the campaign.

[58] The third assumption made in this analysis is that SOA yields do not change on weekends when NO_x concentrations are lower. To test the impact of this assumption, the branching ratios for the high-NO_x and low-NO_x VOC oxidation channels were calculated following the same method as described in *Dzepina et al*. [2011]. It is found that the high-NO_x channel dominates on both weekdays and Sundays with mean branching ratios of 99% and 91%, respectively (see section F of the supporting information for box-and-whiskers plots). Using the NO_x-dependent yields of *Tsimpidi et al*. [2010], this difference in branching ratio would correspond to an increase in weekend SOA yields of 1% (assuming a $7\ \mu g/m^3$ OA concentration) for the aromatic precursors that dominate SOA formation from VOCs [*Dzepina et al*., 2011; *Dzepina et al*., 2009]. This difference in yields would only change the determined diesel contribution by about 2%, which is much smaller than our reported uncertainty. Thus, the assumption that SOA yields do not change on weekends is robust. However, it should be noted that primary semivolatile and intermediate volatility compounds may have an important contribution to SOA formation in the South Coast Air Basin [*Robinson et al*., 2007], but their NO_x-dependent SOA yields are not well constrained.

4. Conclusions

[59] Ambient aerosol measurements were made using a suite of aerosol composition instruments, including online and off-line bulk and single particle methods at the Pasadena ground site during May and June 2010 as part of the CalNex campaign. Organic aerosols account for 41% of the total submicron aerosol mass. An in-depth analysis of OA in Pasadena was carried out including a comparison to measurements from previous field campaigns. Positive matrix factorization analysis of the high-resolution mass spectra resolved five components from the total organic mass. The identified components are hydrocarbon-like organic aerosol (HOA, primary combustion), cooking-influenced organic aerosol (CIOA), semivolatile oxygenated organic aerosol (SV-OOA, fresh secondary), low volatility oxygenated organic aerosol (LV-OOA, aged secondary), and amine-rich local organic aerosol (LOA) that accounts for a small amount of the OA mass. A large majority of the OA mass is classified as oxygenated/secondary (66%), but there are important contributions from the primary components with HOA and CIOA accounting for 12% and 17% of the total OA mass, respectively. To compare the OA oxidation reactions occurring in different regions of the South Coast Air Basin, the Van Krevelen diagrams for Pasadena and Riverside are analyzed and it is observed that OOA components follow a similar line with a slope of −0.55.

[60] The HOA component correlates well with EC, and the emission ratio of HOA to EC varies with the relative importance of diesel versus gasoline vehicle emissions at the Pasadena ground site. The dependence of secondary organic aerosol concentration on photochemical oxidation is quantitatively similar to other urban field sites suggesting similar SOA chemistry and sources. First, the OA to ΔCO ratios for Pasadena increase with photochemical age and closely resemble the upper limit of analogous data from Mexico City and the northeastern United States. Thus, within experimental error, the OA production per unit CO is the same in Pasadena compared to other locations. Second, the OOA to odd-oxygen ratios for Pasadena are similar to those observed in Riverside and Mexico City, which indicates that SOA and odd-oxygen production rates are proportional across the different sites. Both HOA and EC exhibit weekly cycles with substantially lower concentrations on Sundays versus weekdays consistent with the well-known weekday/weekend effect in the South Coast Air Basin. The decreases in HOA and EC concentrations are quantitatively similar to those predicted for their emissions using fuel sales, traffic counts, and literature vehicle emission ratios. In contrast, OOA does not display a strong weekly cycle—after controlling for differences in photochemical ages—which is consistent with the dominance of gasoline emissions in SOA formation, insofar as nonvehicular emissions of SOA precursors are

minor. In total, the findings reported here highlight several quantitative similarities in SOA properties observed in Pasadena, Riverside, Mexico City, and the northeastern United States including the ratios of SOA to odd-oxygen, the increases in OA/ΔCO with photochemical age, and the evolution of elemental composition. These observations are consistent with a relatively constant mix of sources of CO, O_3 precursors, and SOA precursors across urban locations in North America.

Appendix A: Size Distributions, Chemical Aging of Sea Salt, and Particulate Charge Balance

[61] Displayed in Figure A1 are the AMS size distributions (Figure A1a), XRF size distributions (Figure A1c), and the contribution of all species to the total aerosol mass as a function of particle size (Figure A1d). The rBC size distribution was measured by the SP-AMS and is normalized to the total EC concentration measured by the online Sunset analyzer. As seen in Figure A1d, the smaller particles, especially those below 200 nm, are predominately composed of OA. In contrast, the larger particles have an increasing inorganic contribution due to nitrate, sulfate, ammonium, and the non-EC refractory components. The AMS size distributions have a gradual cut of approximately PM_1 and can have a tail due to slow evaporating particles [*Canagaratna et al*., 2004] and should be interpreted accordingly. Also shown in Figure A1e are the PALMS size distributions, which feature a broad submicron mode that is dominated by the sulfate/organic/nitrate particle type as well as a supermicron mode composed primarily of sea salt. The PALMS distributions above 2.5 μm and below 200 nm underestimate concentrations due to instrument limitations associated with both the PALMS and WLOPC.

[62] Further information about the OA, nitrate, and sulfate size distributions can be inferred from comparisons of various PM_1 and $PM_{2.5}$ measurements. For sulfate and OA, the comparisons indicate that on average, an overwhelming majority of the mass for these species is below 1 μm, but for nitrate, there appears to be a substantial amount mass above 1 μm. Specifically, a regression analysis of OC concentrations from the AMS, a PM_1 instrument, and several $PM_{2.5}$ OC time series taken from the GIT, EPA, and UNC filter samples results in slopes greater than 0.81, when the AMS data are plotted on the *y* axis (supporting information section B contains further details about the OA, sulfate, and nitrate comparisons). This observation indicates that less than about 20% of the OC mass is above 1 μm. Similarly, a regression analysis of sulfate concentrations from the AMS and a $PM_{2.5}$ PILS-IC instrument results in slope of 1.01 leading to the conclusion that the sulfate mass above 1 μm is insignificant on average. The regression analysis of AMS and PILS-IC concentration data for nitrate results in a much different finding and exhibits slope of 0.64 that is also dependent on sea-salt concentrations measured by the PALMS instrument. These observations indicate that a substantial amount of nitrate mass is present above 1 μm, about 35%, and that the supermicron nitrate is at least partially comprised of sodium nitrate from chemical aging of sea salt by nitric acid although some supermicron ammonium nitrate may be present as well. The PILS-IC inlet was alternated between PM_1 and $PM_{2.5}$ cyclones for a portion of the measurement period (12–16 June), which provides data that can also be used to assess the amount of sulfate and nitrate between 1 and 2.5 μm. The linear regressions of the PM_1 and linearly interpolated $PM_{2.5}$ data indicate that 34% and 80% of the nitrate and sulfate mass were present below 1 μm. (Note: Interpolation of the $PM_{2.5}$ data is necessary since only a single inlet and cyclone were used for the PILS-IC measurement preventing simultaneous measurements with different size cuts.) Similar to the AMS versus PILS comparison, these percentages indicate that the supermicron mass represents a greater fraction of the $PM_{2.5}$ mass for nitrate relative to sulfate. When using the PILS data with alternating cyclones, a larger percentage of supermicron mass is found than in the AMS versus PILS comparison. This difference may be due to the stronger influence of sea salt during the portion of the campaign when the cyclones were alternated, as clearly seen in the PALMS time series (Figure 1e), which is consistent with substantial amounts of sodium nitrate, and to a lesser extent sodium sulfate, above 1 μm. The aging of sea salt upon exposure to pollution is described further in the next paragraph.

[63] Both the CalNex XRF and PALMS measurements provide quantitative information about non-EC refractory materials including sea salt. An important detail regarding the measurement of particulate chloride is that XRF is assumed to measure refractory chloride (rCl) since the XRF samples are placed under vacuum before measurements [*Johnson et al*., 2008]. The nonrefractory and refractory chloride fractions are thought to be predominately ammonium chloride [*Salcedo et al*., 2006] and sodium chloride (from sea salt), respectively [*Malm et al*., 1994; *Simon et al*., 2011]. Sodium data are not available from XRF due to measurement limitations, but the sodium mass concentration can be estimated from PALMS sea-salt volume concentrations as described in the Figure 2 caption. For fresh sea salt, the expected ratio of chloride to sodium mass concentrations is 1.8 [*Finlayson-Pitts and Pitts*, 2000]. However, a ratio of 0.12 is observed for rCl to sodium at the Pasadena ground site indicating that the sodium chloride in sea-salt aerosol has undergone a substantial amount of chemical processing by nitric and sulfuric acid, which depletes the amount of chloride ions in the sea-salt aerosol by converting sodium chloride to sodium nitrate and sodium sulfate [*Gard et al*., 1998]. For Pasadena, a fractional chloride depletion of 94% is calculated using the following equation described by *Zhuang et al*. [1999]. (In equation (A1), all concentrations are in units of mol m^{-3}.)

$$Depletion = \frac{[Cl]_{\text{original}} - [Cl]}{[Cl]_{\text{original}}} \times 100\% = \frac{1.174[Na] - [Cl]}{1.174[Na]} \times 100\% \quad \text{(A1)}$$

[64] This agrees with qualitative results from the PALMS mass spectra, which show significant displacement of chloride and accumulation of nitrate on individual sea-salt particles that correlated with nitric acid concentrations.

[65] The acidity of the submicron aerosols in Pasadena can be evaluated by comparing the measured ammonium mass concentration against the amount needed to fully neutralize the measured sulfate, nitrate, and chloride, which is termed here

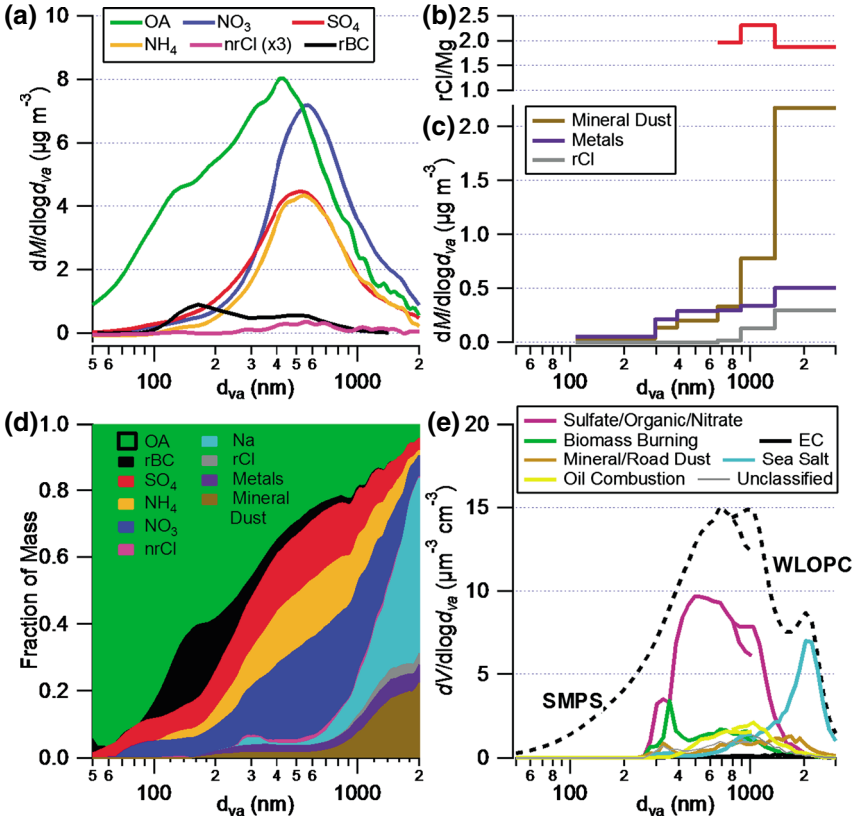

Figure A1. (a) Size distributions measured by the AMS. Also shown is rBC measured by the SP-AMS. Note: The AMS size distributions have a gradual cut of approximately PM_1 and can have a tail due to slow evaporating particles and should be interpreted accordingly. (b) The ratio of rCl to Mg plotted versus particle size. Ratio is calculated using mass concentrations from XRF for 20 May 00:00 to 25 May 00:00. (c) Distribution for refractory components measured by XRF. (d) PM_1 size distributions by percent mass. The XRF data are calculated by interpolating the original data to provide sufficient data points to create the stacked plot. Note: rBC concentrations below 100 nm may be underestimated due to instrument limitations. Sodium is estimated from the PALMS data as described in the Figure 2 caption. (e) Distributions of particle types measured by the PALMS. Volume distributions determined from the SMPS and WLOPC are shown as well. For the size range overlap of the SMPS and WLOPC, each particle type has two data points in each size bin, which is due to mapping the PALMS particle fractions onto the two sizing instruments.

"NH_4^+ predicted." The AMS measurements of nonrefractory aerosol composition were used for this charge balance calculation. Particles are considered acidic if the measured ammonium concentration is substantially lower than the predicted values [*Zhang et al.*, 2007a]. As seen in Figure A2a, overall, the particles appear to be bulk neutralized by ammonium with a majority of the data near the one-to-one line. It should be noted that the measured amines are not accounted for in the predicted ammonium, but even if it is assumed that the amines are all present as salts, the impact on the fit is minimal with the slope changing from 1.02 to 0.99 or 0.96 when AMS or FTIR measurements of amines are used, respectively. There are selected periods when the measured ammonium concentrations are not sufficient to neutralize the anions, especially at lower concentrations. These periods are more easily observed in the histogram shown in Figure A2b. The low ammonium measured-to-predicted ratios may be due to more acidic particles, but based on PALMS spectra only, about 0.1% of particles contained sulfate that was highly acidic ($NH_4^+ : SO_4^{2-} < 1$) [*Froyd et al.*, 2009]. An alternative explanation then is the presence of sodium cations that are not accounted for in Figures A2a and A2b. Typically when using AMS data to evaluate particle acidity, it must be assumed that ammonium is the only significant cation, and cations from sources such as sea salt are ignored [*Aiken et al.*, 2009; *Docherty et al.*, 2011; *Zhang et al.*, 2007a]. For Pasadena, however, sodium concentration data can be estimated from PALMS measurements providing an opportunity to evaluate the role of sea salt in particle neutralization. (Note: The PALMS data were restricted to the submicron size range to match the AMS measurements.) In Figure A2c, there is a clear dependence of the ammonium measured-to-predicted ratios on the fraction of cations that are sodium (ratios are taken from molar units), which indicates that sodium plays a role in the charge balance.

[66] An important consideration when evaluating particle neutralization is whether the sodium cations are present as sodium nitrate or sodium chloride, and if those species can be vaporized by the AMS heater for detection. From the charge balance calculations above, it appears that anions associated with sodium are detected by the AMS indicating that at least a fraction of the sodium nitrate evaporates

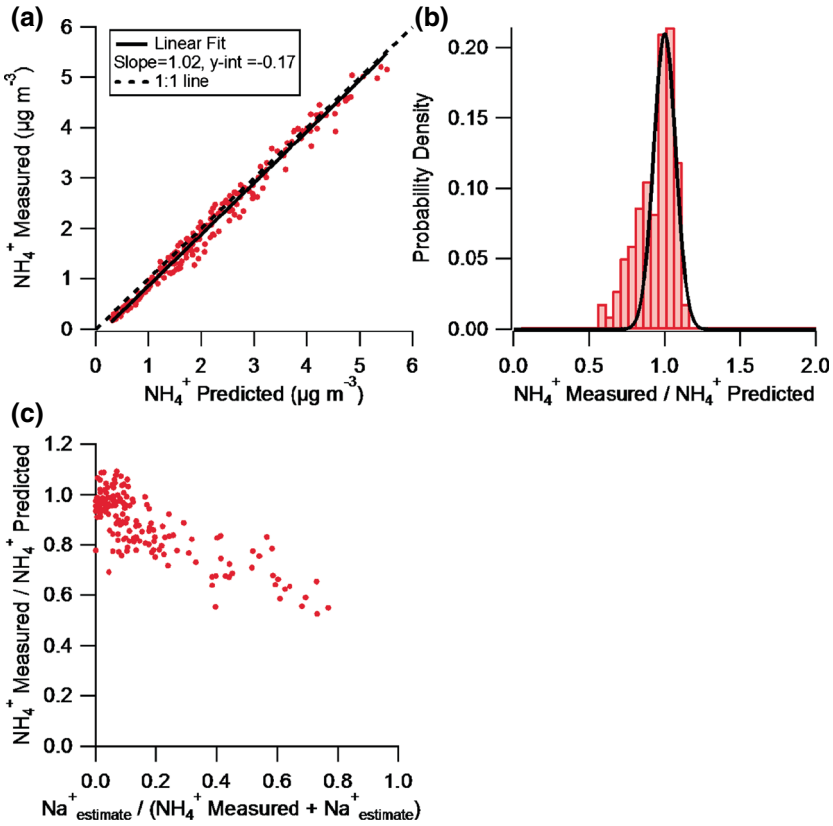

Figure A2. (a) Scatter plot of the measured ammonium versus "NH_4^+ predicted," which is calculated using the concentrations of nitrate, sulfate, and chloride, as well as assuming full neutralization by ammonium (all data from AMS). (b) Histogram for the ratios of the measured ammonium to the NH_4^+ predicted. A Gaussian distribution is shown in the histogram for reference and is generated using the standard deviation of the data. (c) Scatter plot of the measured-to-predicted ratios versus the ratios of sodium to the total cations (ammonium plus sodium). Sodium is estimated from the PALMS sea-salt concentrations as described in the Figure 2 caption.

rapidly (~1 s) in the AMS. The chloride depletion results indicate that a large majority of the sodium is present as sodium nitrate, which is more volatile than sodium chloride and, thus, more readily detected by the AMS, in which the vaporizer temperature was operated at approximately 600 °C. Therefore, it appears that counter ions associated with sodium from sea salt do impact the AMS measurements of charge balance.

[67] Previously, *Docherty et al*. [2011] demonstrated that for Riverside during the SOAR-1 campaign, organonitrates and organosulfates impacted the charge balance calculation. These species add to the nitrate and sulfate mass measured by the AMS [*Farmer et al*., 2010] due to fragmentation of the molecular parent, but do not contribute the expected amount of ionic charge, which leads to apparent particle acidity. An important contrast between Pasadena and Riverside is that the deviation between measured ammonium and NH_4^+ predicted occurs at low concentrations for Pasadena but at high concentrations for Riverside. In addition, the measured versus predicted scatter plot for Pasadena has slope close to one, 1.02, whereas the analogous plot for Riverside has a lower slope of 0.86. (Note: Sodium from sea salt is not accounted for in either slope.) For Riverside, the deviation in the slope from one was attributed to organosulfates and organonitrates. For Pasadena, the charge balance calculation does not appear to be significantly impacted by organosulfates or organonitrates, which implies that the concentrations for these species are relatively low. This conclusion is supported by measurements from other instruments. The PALMS instrument observed that the isoprene-derived organosulfate, IEPOX sulfate ester, comprised <0.01% of submicron aerosol mass in Pasadena, which supports the negligible role of organosulfates in this location. (Note: The mass abundance for the IEPOX sulfate ester was determined using detailed laboratory calibrations that were performed for a previous study [*Froyd et al*., 2010].) Furthermore, FTIR measurements of organonitrates [*Day et al*., 2010] found that concentrations were less than 2% of the measured nitrate (by AMS) on average, which is much lower than the percentage estimated in Riverside (10%).

[68] Combining the discussions of size distributions and sea salt aging from above, in Figure A1b the rCl to Mg ratio is shown as function of particle size for the period of high marine influence identified in section 3.1 (20–25 May 2010). During this period, rCl and Mg are correlated in the larger XRF size bins ($R > 0.62$), and the ratio of the Mg PM_1 mass concentration to the PALMS sea-salt PM_1 mass concentration is very close to the expected ratio for sea salt: 0.044 versus 0.039, respectively ($R = 0.6$) [*Finlayson-Pitts and Pitts*, 2000]. Thus, Mg is taken to be predominately from sea salt, which allows for calculating the amount of chloride depletion following an approach analogous to that described for sodium.

(Data are not shown for smaller particle diameters since a strong correlation between rCl and Mg is not observed.) The rCl to Mg ratio is fairly constant with particle size from 660 to 3010 nm d_{va} indicating similar amounts of chloride depletion. Additionally, the average rCl to Mg ratio (2.0) corresponds to 86% chloride depletion, which is similar to 94% chloride depletion calculated using the estimated sodium data from the PALMS instrument. In general, the sea salt measured in Pasadena appears to be very aged mostly from chemical reactions with nitric acid. The extensive chloride depletion observed in Pasadena is consistent with previous work including modeling studies that predicted ~80% chloride depletion in Riverside, CA [*Knipping and Dabdub*, 2003], and single particle mass spectra of aged sea salt, also from Riverside, which showed extensive chloride depletion [*Hughes et al.*, 2000]. In addition, chloride depletions of 71 and 74% were reported for coarse mode aerosol in Upland and Rubidoux, CA, respectively [*Eldering et al.*, 1991]. These values are lower than that observed for Pasadena in this study, which may be due to the Eldering et al. percentages corresponding to particles greater than 2.2 μm in diameter.

[69] The extensive depletion of chloride from sea salt suggests that appreciable amounts of chlorine radicals may be present due to the photolysis of photolabile chlorinated gases such as HCl, $ClNO_2$, and Cl_2. Oxidation reactions of organics by chlorine radicals that produce organochlorines in the particle phase would then be possible. To investigate this possibility, the concentrations of several organochlorine fragments were determined from the AMS measurements (CCl^+, C_2HCl^+, CCl_2^+, $C_2Cl_2^+$, $C_2HCl_2^+$, $CHOCl_2^+$). The relative concentration of these species compared to the total OA is very small, on average less than 0.1% and always less than 0.4%. In addition, the 2DTAG identified only one chlorine-containing OA compound, chlorophthalic acid, which represents less than 1% of the total phthalic acid concentration. These results are also consistent with FTIR spectra of filter samples collected during the CalNex campaign, which do not display vibrational resonances for acid chlorides (730–550 cm^{-1}) or alkyl chlorides (785–540 cm^{-1}). It is noted though that quantification of organochlorines by FTIR is difficult due to Teflon filter interferences in the same spectral region. In total, these measurements provide no evidence for organochlorines representing a substantial portion of the OA mass, but the methods utilized here are not optimal for the detection of organochlorines.

[70] **Acknowledgments.** The authors thank Jochen Stutz and John Seinfeld for their leadership in organizing the Pasadena ground site, and CARB and NOAA for support of the site setup. We also wish to thank Ingrid Ulbrich for helpful discussions regarding the PMF analysis and Cora Young for providing radical budgets for the CalNex ground site. The Jimenez Group acknowledges support from CARB 08-319 and CARB 11-305 as well as DOE (BER, ASR Program) DE-SC0006035, DE-SC0006711, and DE-FG02-11ER65293. PLH and AMO acknowledge fellowships from the CIRES Visiting Fellows Program and US DOE SCGF Program (ORAU, ORISE, DE-AC05-06OR23100), respectively. JT and JDA acknowledge funding from the Natural Environment Research Council [Ref: NE/H008136/1]. RJW and XZ were funded through National Science Foundation grants ATM-0931492 and ATM-0802237. ALC acknowledges fellowship support from US DOE SCGF Program (ORAU, ORISE, DE-AC05-06OR23100) and other expenses from NSF grant AGS-1009408. YZ and SSC acknowledge support from CARB 09-350. The U.S. Environmental Protection Agency (EPA) through its Office of Research and Development collaborated in the research described here; the manuscript has been subjected to peer review and has been cleared for publication; mention of trade names or commercial products does not constitute endorsement or recommendation for use by the EPA.

References

Aiken, A. C., P. F. DeCarlo, and J. L. Jimenez (2007), Elemental analysis of organic species with electron ionization high-resolution mass spectrometry, *Anal. Chem.*, *79*(21), 8350–8358.

Aiken, A. C., et al. (2008), O/C and OM/OC ratios of primary, secondary, and ambient organic aerosols with high-resolution time-of-flight aerosol mass spectrometry, *Environ. Sci. Technol.*, *42*(12), 4478–4485.

Aiken, A. C., et al. (2009), Mexico City aerosol analysis during MILAGRO using high resolution aerosol mass spectrometry at the urban supersite (T0)—Part 1: Fine particle composition and organic source apportionment, *Atmos. Chem. Phys.*, *9*(17), 6633–6653.

Aiken, A. C., et al. (2010), Mexico City aerosol analysis during MILAGRO using high resolution aerosol mass spectrometry at the urban supersite (T0)—Part 2: Analysis of the biomass burning contribution and the non-fossil carbon fraction, *Atmos. Chem. Phys.*, *10*(12), 5315–5341.

Allan, J. D., et al. (2003), Quantitative sampling using an Aerodyne aerosol mass spectrometer: 2. Measurements of fine particulate chemical composition in two UK cities, *J. Geophys. Res.*, *108*(D3), 4091, doi:10.1029/2002JD002359.

Allan, J. D., et al. (2004), A generalised method for the extraction of chemically resolved mass spectra from Aerodyne aerosol mass spectrometer data, *J. Aerosol. Sci.*, *35*(7), 909–922.

Allan, J. D., P. I. Williams, W. T. Morgan, C. L. Martin, M. J. Flynn, J. Lee, E. Nemitz, G. J. Phillips, M. W. Gallagher, and H. Coe (2010), Contributions from transport, solid fuel burning and cooking to primary organic aerosols in two UK cities, *Atmos. Chem. Phys.*, *10*(2), 647–668.

Apel, E. C., et al. (2010), Chemical evolution of volatile organic compounds in the outflow of the Mexico City metropolitan area, *Atmos. Chem. Phys.*, *10*(5), 2353–2375.

Ault, A. P., M. J. Moore, H. Furutani, and K. A. Prather (2009), Impact of emissions from the Los Angeles port region on San Diego air quality during regional transport events, *Environ. Sci. Technol.*, *43*(10), 3500–3506.

Bahreini, R., et al. (2012), Gasoline emissions dominate over diesel in formation of secondary organic aerosol mass, *Geophys. Res. Lett.*, *39*, L06805, doi:10.1029/2011GL050718.

Ban-Weiss, G. A., J. P. McLaughlin, R. A. Harley, A. J. Kean, E. Grosjean, and D. Grosjean (2008a), Carbonyl and nitrogen dioxide emissions from gasoline- and diesel-powered motor vehicles, *Environ. Sci. Technol.*, *42*(11), 3944–3950.

Ban-Weiss, G. A., J. P. McLaughlin, R. A. Harley, M. M. Lunden, T. W. Kirchstetter, A. J. Kean, A. W. Strawa, E. D. Stevenson, and G. R. Kendall (2008b), Long-term changes in emissions of nitrogen oxides and particulate matter from on-road gasoline and diesel vehicles, *Atmos. Environ.*, *42*(2), 220–232.

Bhattacharya, S. C., D. O. Albina, and P. A. Salam (2002), Emission factors of wood and charcoal-fired cookstoves, *Biomass Bioenergy*, *23*(6), 453–469.

Blumenthal, D. L., W. H. White, and T. B. Smith (1978), Anatomy of a Los Angeles smog episode—Pollutant transport in daytime sea breeze regime, *Atmos. Environ.*, *12*(4), 893–907.

Bon, D. M., et al. (2011), Measurements of volatile organic compounds at a suburban ground site (T1) in Mexico City during the MILAGRO 2006 campaign: Measurement comparison, emission ratios, and source attribution, *Atmos. Chem. Phys.*, *11*(6), 2399–2421.

Brioude, J., W. M. Angevine, S. A. McKeen, and E. Y. Hsie (2012), Numerical uncertainty at mesoscale in a Lagrangian model in complex terrain, *Geosci. Model Dev.*, *5*(5), 1127–1136.

Canagaratna, M. R., et al. (2004), Chase studies of particulate emissions from in-use New York City vehicles, *Aerosol Sci. Technol.*, *38*(6), 555–573.

Cappa, C. D., and J. L. Jimenez (2010), Quantitative estimates of the volatility of ambient organic aerosol, *Atmos. Chem. Phys.*, *10*(12), 5409–5424.

Chang, W. L., P. V. Bhave, S. S. Brown, N. Riemer, J. Stutz, and D. Dabdub (2011), Heterogeneous atmospheric chemistry, ambient measurements, and model calculations of N2O5: A review, *Aerosol Sci. Technol.*, *45*(6), 665–695.

Chinkin, L. R., D. L. Coe, T. H. Funk, H. R. Hafner, P. T. Roberts, P. A. Ryan, and D. R. Lawson (2003), Weekday versus weekend activity patterns for ozone precursor emissions in California's South Coast Air Basin, *J. Air Waste Manage. Assoc.*, *53*(7), 829–843.

Crippa, M., et al. (2013), Wintertime aerosol chemical composition and source apportionment of the organic fraction in the metropolitan area of Paris, *Atmos. Chem. Phys.*, *13*(2), 961–981.

Croes, B. E., and E. M. Fujita (2003), Overview of the 1997 Southern California Ozone Study (SCOS97-NARSTO), *Atmos. Environ.*, *37*, S3–S26.

Cubison, M. J., et al. (2011), Effects of aging on organic aerosol from open biomass burning smoke in aircraft and laboratory studies, *Atmos. Chem. Phys.*, *11*(23), 12,049–12,064.

Day, D. A., S. Liu, L. M. Russell, and P. J. Ziemann (2010), Organonitrate group concentrations in submicron particles with high nitrate and organic fractions in coastal southern California, *Atmos. Environ.*, *44*(16), 1970–1979.

DeCarlo, P. F., et al. (2006), Field-deployable, high-resolution, time-of-flight aerosol mass spectrometer, *Anal. Chem.*, *78*, 8281–8289.

DeCarlo, P. F., et al. (2010), Investigation of the sources and processing of organic aerosol over the Central Mexican Plateau from aircraft measurements during MILAGRO, *Atmos. Chem. Phys.*, *10*(12), 5257–5280.

de Gouw, J. A., et al. (2012), Increasing atmospheric burden of ethanol in the United States, *Geophys. Res. Lett.*, *39*, L15803, doi:10.1029/2012GL052109.

Docherty, K. S., et al. (2008), Apportionment of primary and secondary organic aerosols in southern California during the 2005 study of organic aerosols in riverside (SOAR-1), *Environ. Sci. Technol.*, *42*(20), 7655–7662.

Docherty, K. S., et al. (2011), The 2005 study of organic aerosols at riverside (SOAR-1): Instrumental intercomparisons and fine particle composition, *Atmos. Chem. Phys.*, *11*(23), 12,387–12,420.

Dockery, D. W., and C. A. Pope (1994), Acute respiratory effects of particulate air-pollution, *Annu. Rev. Public Health*, *15*, 107–132.

Dockery, D. W., C. A. Pope, X. P. Xu, J. D. Spengler, J. H. Ware, M. E. Fay, B. G. Ferris, and F. E. Speizer (1993), An association between air-pollution and mortality in six U.S. cities, *N. Engl. J. Med.*, *329*(24), 1753–1759.

Dunlea, E. J., et al. (2009), Evolution of Asian aerosols during transpacific transport in INTEX-B, *Atmos. Chem. Phys.*, *9*(19), 7257–7287.

Dusanter, S., D. Vimal, P. S. Stevens, R. Volkamer, and L. T. Molina (2009), Measurements of OH and HO2 concentrations during the MCMA-2006 field campaign—Part 1: Deployment of the Indiana University laser-induced fluorescence instrument, *Atmos. Chem. Phys.*, *9*(5), 1665–1685.

Dzepina, K., R. M. Volkamer, S. Madronich, P. Tulet, I. M. Ulbrich, Q. Zhang, C. D. Cappa, P. J. Ziemann, and J. L. Jimenez (2009), Evaluation of recently-proposed secondary organic aerosol models for a case study in Mexico City, *Atmos. Chem. Phys.*, *9*(15), 5681–5709.

Dzepina, K., C. D. Cappa, R. M. Volkamer, S. Madronich, P. F. DeCarlo, R. A. Zaveri, and J. L. Jimenez (2011), Modeling the multiday evolution and aging of secondary organic aerosol during MILAGRO 2006, *Environ. Sci. Technol.*, *45*(8), 3496–3503.

Eldering, A., P. A. Solomon, L. G. Salmon, T. Fall, and G. R. Cass (1991), Hydrochloric acid—A regional perspective on concentrations and formation in the atmosphere of southern California, *Atmos. Environ. Part A*, *25*(10), 2091–2102.

Farmer, D. K., A. Matsunaga, K. S. Docherty, J. D. Surratt, J. H. Seinfeld, P. J. Ziemann, and J. L. Jimenez (2010), Response of an aerosol mass spectrometer to organonitrates and organosulfates and implications for atmospheric chemistry, *Proc. Natl. Acad. Sci. U.S.A.*, *107*(15), 6670–6675.

Finlayson-Pitts, B. J., and J. N. Pitts (2000), *Chemistry of the Upper and Lower Atmosphere*, Academic, San Diego, Calif.

Froyd, K. D., D. M. Murphy, T. J. Sanford, D. S. Thomson, J. C. Wilson, L. Pfister, and L. Lait (2009), Aerosol composition of the tropical upper troposphere, *Atmos. Chem. Phys.*, *9*(13), 4363–4385.

Froyd, K. D., S. M. Murphy, D. M. Murphy, J. A. de Gouw, N. C. Eddingsaas, and P. O. Wennberg (2010), Contribution of isoprene-derived organosulfates to free tropospheric aerosol mass, *Proc. Natl. Acad. Sci. U.S.A.*, *107*(50), 21,360–21,365.

Fruin, S. A., M. J. St Denis, A. M. Winer, S. D. Colome, and F. W. Lurmann (2001), Reductions in human benzene exposure in the California South Coast Air Basin, *Atmos. Environ.*, *35*(6), 1069–1077.

Gard, E. E., et al. (1998), Direct observation of heterogeneous chemistry in the atmosphere, *Science*, *279*(5354), 1184–1187.

Gentner, D. R., et al. (2012), Elucidating secondary organic aerosol from diesel and gasoline vehicles through detailed characterization of organic carbon emissions, *Proc. Natl. Acad. Sci. U. S. A.*, *109*(45), 18,318–18,323.

Gerbig, C., S. Schmitgen, D. Kley, A. Volz-Thomas, K. Dewey, and D. Haaks (1999), An improved fast-response vacuum-UV resonance fluorescence CO instrument, *J. Geophys. Res.*, *104*(D1), 1699–1704.

Gilman, J. B., et al. (2009), Measurements of volatile organic compounds during the 2006 TexAQS/GoMACCS campaign: Industrial influences, regional characteristics, and diurnal dependencies of the OH reactivity, *J. Geophys. Res.*, *114*, D00F06, doi:10.1029/2008JD011525.

Griffin, R. J., J. J. Chen, K. Carmody, S. Vutukuru, and D. Dabdub (2007), Contribution of gas phase oxidation of volatile organic compounds to atmospheric carbon monoxide levels in two areas of the United States, *J. Geophys. Res.*, *112*, D10S17, doi:10.1029/2006JD007602.

Hall, J. S., and E. W. Wolff (1998), Causes of seasonal and daily variations in aerosol sea-salt concentrations at a coastal Antarctic station, *Atmos. Environ.*, *32*(21), 3669–3677.

Haman, C. L., B. Lefer, and G. A. Morris (2012), Seasonal variability in the diurnal evolution of the boundary layer in a near coastal urban environment, *J. Atmos. Oceanic Technol.*, *29*(5), 97–710.

Harley, R. A., R. F. Sawyer, and J. B. Milford (1997), Updated photochemical modeling for California's South Coast Air Basin: Comparison of chemical mechanisms and motor vehicle emission inventories, *Environ. Sci. Technol.*, *31*(10), 2829–2839.

Heald, C. L., J. H. Kroll, J. L. Jimenez, K. S. Docherty, P. F. DeCarlo, A. C. Aiken, Q. Chen, S. T. Martin, D. K. Farmer, and P. Artaxo (2010), A simplified description of the evolution of organic aerosol composition in the atmosphere, *Geophys. Res. Lett.*, *37*, L08803, doi:10.1029/2010GL042737.

Healy, R. M., I. P. O'Connor, S. Hellebust, A. Allanic, J. R. Sodeau, and J. C. Wenger (2009), Characterisation of single particles from in-port ship emissions, *Atmos. Environ.*, *43*(40), 6408–6414.

Herndon, S. C., et al. (2008), Correlation of secondary organic aerosol with odd oxygen in Mexico City, *Geophys. Res. Lett.*, *35*, L15804, doi:10.1029/2008GL034058.

Hersey, S. P., J. S. Craven, K. A. Schilling, A. R. Metcalf, A. Sorooshian, M. N. Chan, R. C. Flagan, and J. H. Seinfeld (2011), The Pasadena Aerosol Characterization Observatory (PACO): Chemical and physical analysis of the Western Los Angeles basin aerosol, *Atmos. Chem. Phys.*, *11*(15), 7417–7443.

Hildebrandt, L., E. Kostenidou, V. A. Lanz, A. S. H. Prevot, U. Baltensperger, N. Mihalopoulos, A. Laaksonen, N. M. Donahue, and S. N. Pandis (2011), Sources and atmospheric processing of organic aerosol in the Mediterranean: Insights from aerosol mass spectrometer factor analysis, *Atmos. Chem. Phys.*, *11*(23), 12,499–12,515.

Hildemann, L. M., G. R. Markowski, and G. R. Cass (1991), Chemical-composition of emissions from urban sources of fine organic aerosol, *Environ. Sci. Technol.*, *25*(4), 744–759.

Hodzic, A., and J. L. Jimenez (2011), Modeling anthropogenically controlled secondary organic aerosols in a megacity: A simplified framework for global and climate models, *Geosci. Model Dev.*, *4*, 901–917.

Hodzic, A., J. L. Jimenez, A. S. H. Prevot, S. Szidat, J. D. Fast, and S. Madronich (2010), Can 3-D models explain the observed fractions of fossil and non-fossil carbon in and near Mexico City?, *Atmos. Chem. Phys.*, *10*(22), 10,997–11,016.

Huang, X. F., et al. (2010), Highly time-resolved chemical characterization of atmospheric submicron particles during 2008 Beijing Olympic Games using an Aerodyne High-Resolution Aerosol Mass Spectrometer, *Atmos. Chem. Phys.*, *10*(18), 8933–8945.

Huffman, J. A., et al. (2009), Chemically-resolved aerosol volatility measurements from two megacity field studies, *Atmos. Chem. Phys.*, *9*(18), 7161–7182.

Hughes, L. S., J. O. Allen, P. Bhave, M. J. Kleeman, G. R. Cass, D. Y. Liu, D. F. Fergenson, B. D. Morrical, and K. A. Prather (2000), Evolution of atmospheric particles along trajectories crossing the Los Angeles basin, *Environ. Sci. Technol.*, *34*(15), 3058–3068.

International Panel on Climate Change (2007), *Climate Change 2007: The Physical Scientific Basis*, Cambridge Univ. Press, Cambridge, U. K.

Jacob, D. J., et al. (2010), The arctic research of the composition of the troposphere from aircraft and satellites (ARCTAS) mission: Design, execution, and first results, *Atmos. Chem. Phys.*, *10*(11), 5191–5212.

Jimenez, J. L., et al. (2003), Ambient aerosol sampling using the Aerodyne Aerosol Mass Spectrometer, *J. Geophys. Res.*, *108*(D7), 8425, doi:10.1029/2001JD001213.

Jimenez, J. L., et al. (2009), Evolution of organic aerosols in the atmosphere, *Science*, *326*(5959), 1525–1529.

Johnson, K. S., A. Laskin, J. L. Jimenez, V. Shutthanandan, L. T. Molina, D. Salcedo, K. Dzepina, and M. J. Molina (2008), Comparative analysis of urban atmospheric aerosol by particle-induced X-ray emission (PIXE), proton elastic scattering analysis (PESA), and aerosol mass spectrometry (AMS), *Environ. Sci. Technol.*, *42*(17), 6619–6624.

Kebabian, P. L., W. A. Robinson, and A. Freedman (2007), Optical extinction monitor using cw cavity enhanced detection, *Rev. Sci. Instrum.*, *78*(6), 063102, doi:10.1063/1.2744223.

Kleinman, L. I., et al. (2007), Aircraft observations of aerosol composition and ageing in New England and Mid-Atlantic States during the summer 2002 New England Air quality study field campaign, *J. Geophys. Res.*, *112*, D09310, doi:10.1029/2006JD007786.

Kleinman, L. I., et al. (2008), The time evolution of aerosol composition over the Mexico City plateau, *Atmos. Chem. Phys.*, *8*(6), 1559–1575.

Knipping, E. M., and D. Dabdub (2003), Impact of chlorine emissions from sea-salt aerosol on coastal urban ozone, *Environ. Sci. Technol.*, *37*(2), 275–284.

Lambe, A. T., et al. (2012), Transitions from functionalization to fragmentation reactions of laboratory secondary organic aerosol (SOA) generated from the OH oxidation of alkane precursors, *Environ. Sci. Technol.*, *46*(10), 5430–5437.

Langridge, J. M., et al. (2012), Evolution of aerosol properties impacting visibility and direct climate forcing in an ammonia-rich urban environment, *J. Geophys. Res.*, *117*, D00V11, doi:10.1029/2011JD017116.

Lanz, V. A., M. R. Alfarra, U. Baltensperger, B. Buchmann, C. Hueglin, and A. S. H. Prevot (2007), Source apportionment of submicron organic aerosols at an urban site by factor analytical modelling of aerosol mass spectra, *Atmos. Chem. Phys.*, *7*(6), 1503–1522.

Lawson, D. R. (1990), The southern California air-quality study, *J. Air Waste Manage. Assoc.*, *40*(2), 156–165.

Lee, S. C., W. M. Li, and L. Y. Chan (2001), Indoor air quality at restaurants with different styles of cooking in metropolitan Hong Kong, *Sci. Total Environ.*, *279*(1-3), 181–193.

Liu, S., D. A. Day, J. E. Shields, and L. M. Russell (2011), Ozone-driven daytime formation of secondary organic aerosol containing carboxylic acid groups and alkane groups, *Atmos. Chem. Phys.*, *11*(16), 8321–8341.

Lu, R., and R. P. Turco (1995), Air pollutant transport in a coastal environment—II. Three-dimensional simulations over Los Angeles basin, *Atmos. Environ.*, *29*(13), 1499–1518.

Malm, W. C., J. F. Sisler, D. Huffman, R. A. Eldred, and T. A. Cahill (1994), Spatial and seasonal trends in particle concentration and optical extinction in the United States, *J. Geophys. Res.*, *99*(D1), 1347–1370.

Marr, L. C., and R. A. Harley (2002), Spectral analysis of weekday-weekend differences in ambient ozone, nitrogen oxide, and non-methane hydrocarbon time series in California, *Atmos. Environ.*, *36*(14), 2327–2335.

Massoli, P., P. L. Kebabian, T. B. Onasch, F. B. Hills, and A. Freedman (2010), Aerosol light extinction measurements by Cavity Attenuated Phase Shift (CAPS) spectroscopy: Laboratory validation and field deployment of a compact aerosol particle extinction monitor, *Aerosol Sci. Technol.*, *44*(6), 428–435.

McDonald, J. D., B. Zielinska, E. M. Fujita, J. C. Sagebiel, J. C. Chow, and J. G. Watson (2003), Emissions from charbroiling and grilling of chicken and beef, *J. Air Waste Manage. Assoc.*, *53*(2), 185–194.

McLafferty, F. W., and F. Turecek (1993), *Interpretation of Mass Spectra*, 4th ed., Univ. Sci. Books, Sausalito, Calif.

Middlebrook, A. M., R. Bahreini, J. L. Jimenez, and M. R. Canagaratna (2012), Evaluation of composition-dependent collection efficiencies for the Aerodyne aerosol mass spectrometer using field data, *Aerosol Sci. Technol.*, *46*(3), 258–271.

Millstein, D. E., R. A. Harley, and S. V. Hering (2008), Weekly cycles in fine particulate nitrate, *Atmos. Environ.*, *42*(4), 632–641.

Mohr, C., et al. (2011), Identification and quantification of organic aerosol from cooking and other sources in Barcelona using aerosol mass spectrometer data, *Atmos. Chem. Phys.*, *11*(10), 1649–1665.

Moore, G. E., S. G. Douglas, R. C. Kessler, and J. P. Killus (1991), Identification and tracking of polluted air masses in the South-Central Coast Air Basin, *J. Appl. Meteorol.*, *30*(5), 715–732.

Murphy, B. N., N. M. Donahue, C. Fountoukis, and S. N. Pandis (2011), Simulating the oxygen content of ambient organic aerosol with the 2D volatility basis set, *Atmos. Chem. Phys.*, *11*(15), 7859–7873.

National Oceanic and Atmospheric Administration (2008), 2010 CalNex White Paper: Research at the Nexus of Air Quality and Climate Change, Silver Spring, Md. [Available at http://www.esrl.noaa.gov/csd/projects/calnex/whitepaper.pdf.].

Nemitz, E. (2010), Aerosol mass spectrometer network measurements during the EUCAARI/EMEP intensive measurement campaigns, paper presented at Aerodyne Aerosol Mass Spectrometer Users Meeting, Hyytiala, Finland, 4–6 September.

Neuman, J. A., et al. (2003), Variability in ammonium nitrate formation and nitric acid depletion with altitude and location over California, *J. Geophys. Res.*, *108*(D17), 4557, doi:10.1029/2003JD003616.

Ng, N. L., M. R. Canagaratna, J. L. Jimenez, P. S. Chhabra, J. H. Seinfeld, and D. R. Worsnop (2011), Changes in organic aerosol composition with aging inferred from aerosol mass spectra, *Atmos. Chem. Phys.*, *11*(13), 6465–6474.

Onasch, T. B., A. Trimborn, E. C. Fortner, J. T. Jayne, G. L. Kok, L. R. Williams, P. Davidovits, and D. R. Worsnop (2012), Soot particle aerosol mass spectrometer: Development, validation, and initial application, *Aerosol Sci. Technol.*, *46*(7), 804–817.

Orsini, D. A., Y. L. Ma, A. Sullivan, B. Sierau, K. Baumann, and R. J. Weber (2003), Refinements to the particle-into-liquid sampler (PILS) for ground and airborne measurements of water soluble aerosol composition, *Atmos. Environ.*, *37*(9–10), 1243–1259.

Paatero, P., and P. K. Hopke (2003), Discarding or downweighting high-noise variables in factor analytic models, *Anal. Chim. Acta*, *490*(1–2), 277–289.

Paatero, P., and U. Tapper (1994), Positive matrix factorization—A nonnegative factor model with optimal utilization of error-estimates of data values, *Environmetrics*, *5*(2), 111–126.

Parrish, D. D., M. Trainer, D. Hereid, E. J. Williams, K. J. Olszyna, R. A. Harley, J. F. Meagher, and F. C. Fehsenfeld (2002), Decadal change in carbon monoxide to nitrogen oxide ratio in US vehicular emissions, *J. Geophys. Res.*, *107*(D12), 4140, doi:10.1029/2001JD000720.

Parrish, D. D., A. Stohl, C. Forster, E. L. Atlas, D. R. Blake, P. D. Goldan, W. C. Kuster, and J. A. de Gouw (2007), Effects of mixing on evolution of hydrocarbon ratios in the troposphere, *J. Geophys. Res.*, *112*, D10S34, doi:10.1029/2006JD007583.

Peltier, R. E., R. J. Weber, and A. P. Sullivan (2007), Investigating a liquid-based method for online organic carbon detection in atmospheric particles, *Aerosol Sci. Technol.*, *41*(12), 1117–1127.

Pollack, I. B., et al. (2012), Airborne and ground-based observations of a weekend effect in ozone, precursors, and oxidation products in the California south coast Air basin, *J. Geophys. Res.*, *117*, D00V05, doi:10.1029/2011JD016772.

Robinson, A. L., R. Subramanian, N. M. Donahue, A. Bernardo-Bricker, and W. F. Rogge (2006), Source apportionment of molecular markers and organic aerosol. 3. Food cooking emissions, *Environ. Sci. Technol.*, *40*(24), 7820–7827.

Robinson, A. L., N. M. Donahue, M. K. Shrivastava, E. A. Weitkamp, A. M. Sage, A. P. Grieshop, T. E. Lane, J. R. Pierce, and S. N. Pandis (2007), Rethinking organic aerosols: Semivolatile emissions and photochemical aging, *Science*, *315*(5816), 1259–1262.

Russell, L. M., S. Takahama, S. Liu, L. N. Hawkins, D. S. Covert, P. K. Quinn, and T. S. Bates (2009), Oxygenated fraction and mass of organic aerosol from direct emission and atmospheric processing measured on the R/V Ronald Brown during TEXAQS/GoMACCS 2006, *J. Geophys. Res.*, *114*, D00F05, doi:10.1029/2008JD011275.

Russell, L. M., L. N. Hawkins, A. A. Frossard, P. K. Quinn, and T. S. Bates (2010), Carbohydrate-like composition of submicron atmospheric particles and their production from ocean bubble bursting, *Proc. Natl. Acad. Sci. U.S.A.*, *107*(15), 6652–6657.

Ryerson, T. B., et al. (2013), The 2010 California Research at the Nexus of Air Quality and Climate Change (CalNex) field study, *J. Geophys. Res. Atmos.*, *118*, 5890–5866, doi:10.1002/jgrd.50331.

Salcedo, D., et al. (2006), Characterization of ambient aerosols in Mexico City during the MCMA-2003 campaign with aerosol mass spectrometry: Results from the CENICA supersite, *Atmos. Chem. Phys.*, *6*, 925–946.

Schauer, J. J., M. J. Kleeman, G. R. Cass, and B. R. T. Simoneit (1999), Measurement of emissions from air pollution sources. 1. C-1 through C-29 organic compounds from meat charbroiling, *Environ. Sci. Technol.*, *33*(10), 1566–1577.

Schauer, J. J., M. J. Kleeman, G. R. Cass, and B. R. T. Simoneit (2002a), Measurement of emissions from air pollution sources. 5. C-1-C-32 organic compounds from gasoline-powered motor vehicles, *Environ. Sci. Technol.*, *36*(6), 1169–1180.

Schauer, J. J., M. J. Kleeman, G. R. Cass, and B. R. T. Simoneit (2002b), Measurement of emissions from air pollution sources. 4. C-1-C-27 organic compounds from cooking with seed oils, *Environ. Sci. Technol.*, *36*(4), 567–575.

Schwarz, J. P., et al. (2006), Single-particle measurements of midlatitude black carbon and light-scattering aerosols from the boundary layer to the lower stratosphere, *J. Geophys. Res.*, *111*, D16207, doi:10.1029/2006JD007076.

Simon, H., P. V. Bhave, J. L. Swall, N. H. Frank, and W. C. Malm (2011), Determining the spatial and seasonal variability in OM/OC ratios across the US using multiple regression, *Atmos. Chem. Phys.*, *11*(6), 2933–2949.

Slowik, J. G., et al. (2010), Characterization of a large biogenic secondary organic aerosol event from eastern Canadian forests, *Atmos. Chem. Phys.*, *10*(6), 2825–2845.

Stohl, A., C. Forster, A. Frank, P. Seibert, and G. Wotawa (2005), Technical note: The Lagrangian particle dispersion model FLEXPART version 6.2, *Atmos. Chem. Phys.*, *5*, 2461–2474.

Sun, Y. L., et al. (2011), Characterization of the sources and processes of organic and inorganic aerosols in New York City with a high-resolution time-of-flight aerosol mass spectrometer, *Atmos. Chem. Phys.*, *11*(4), 1581–1602.

Thalman, R., and R. Volkamer (2010), Inherent calibration of a blue LED-CE-DOAS instrument to measure iodine oxide, glyoxal, methyl glyoxal, nitrogen dioxide, water vapour and aerosol extinction in open cavity mode, *Atmos. Meas. Tech.*, *3*(6), 1797–1814.

Thomson, D. S., M. E. Schein, and D. M. Murphy (2000), Particle analysis by laser mass spectrometry WB-57 F instrument overview, *Aerosol Sci. Technol.*, *33*(1-2), 153–169.

Tsimpidi, A. P., V. A. Karydis, M. Zavala, W. Lei, L. Molina, I. M. Ulbrich, J. L. Jimenez, and S. N. Pandis (2010), Evaluation of the volatility basis-set approach for the simulation of organic aerosol formation in the Mexico City metropolitan area, *Atmos. Chem. Phys.*, *10*(2), 525–546.

Turpin, B. J., J. J. Huntzicker, S. M. Larson, and G. R. Cass (1991), Los Angeles summer midday particulate carbon—Primary and secondary aerosol, *Environ. Sci. Technol.*, *25*(10), 1788–1793.

Ulbrich, I. M., M. R. Canagaratna, Q. Zhang, D. R. Worsnop, and J. L. Jimenez (2009), Interpretation of organic components from Positive Matrix Factorization of aerosol mass spectrometric data, *Atmos. Chem. Phys.*, *9*(9), 2891–2918.

Ulrickson, B. L., and C. F. Mass (1990), Numerical investigation of mesoscale circulations over the Los Angeles Basin. 2. Synoptic influences and pollutant transport, *Mon. Weather Rev.*, *118*(10), 2162–2184.

Veres, P. R., et al. (2011), Evidence of rapid production of organic acids in an urban air mass, *Geophys. Res. Lett.*, *38*, L17807, doi:10.1029/2011GL048420.

Warneke, C., et al. (2007), Determination of urban volatile organic compound emission ratios and comparison with an emissions database, *J. Geophys. Res.*, *112*, D10S47, doi:10.1029/2006JD007930.

Warneke, C., J. A. de Gouw, J. S. Holloway, J. Peischl, T. B. Ryerson, E. Atlas, D. Blake, M. Trainer, and D. D. Parrish (2012), Multiyear trends in volatile organic compounds in Los Angeles, California: Five decades of decreasing emissions, *J. Geophys. Res.*, *117*, D00V17, doi:10.1029/2012JD017899.

Washenfelder, R. A., et al. (2011), The glyoxal budget and its contribution to organic aerosol for Los Angeles, California, during CalNex 2010, *J. Geophys. Res.*, *116*, D00V02, doi:10.1029/2011JD016314.

Watson, J. G. (2002), Visibility: Science and regulation, *J. Air Waste Manage. Assoc.*, *52*(6), 628–713.

Williams, B. J., A. H. Goldstein, N. M. Kreisberg, S. V. Hering, D. R. Worsnop, I. M. Ulbrich, K. S. Docherty, and J. L. Jimenez (2010), Major components of atmospheric organic aerosol in southern California as determined by hourly measurements of source marker compounds, *Atmos. Chem. Phys.*, *10*(23), 11,577–11,603.

Wonaschutz, A., S. P. Hersey, A. Sorooshian, J. S. Craven, A. R. Metcalf, R. C. Flagan, and J. H. Seinfeld (2011), Impact of a large wildfire on water-soluble organic aerosol in a major urban area: The 2009 station fire in Los Angeles county, *Atmos. Chem. Phys.*, *11*(16), 8257–8270.

Wood, E. C., et al. (2010), Investigation of the correlation between odd oxygen and secondary organic aerosol in Mexico City and Houston, *Atmos. Chem. Phys.*, *10*(18), 8947–8968.

Worton, D. R., N. M. Kreisberg, G. Isaacman, A. P. Teng, C. McNeish, T. Górecki, S. V. Hering, and A. H. Goldstein (2012), Thermal desorption comprehensive two-dimensional gas chromatography: An improved instrument for in-situ speciated measurements of organic aerosols, *Aerosol Sci. Technol.*, *46*(4), 380–393.

Young, C. J., et al. (2012), Vertically resolved measurements of nighttime radical reservoirs in Los Angeles and their contribution to the urban radical budget, *Environ. Sci. Technol.*, *46*(20), 10,965–10,973.

Zelenyuk, A., Y. Cai, L. Chieffo, and D. Imre (2005), High precision density measurements of single particles: The density of metastable phases, *Aerosol Sci. Technol.*, *39*(10), 972–986.

Zhang, Q., J. L. Jimenez, D. R. Worsnop, and M. Canagaratna (2007a), A case study of urban particle acidity and its influence on secondary organic aerosol, *Environ. Sci. Technol.*, *41*(9), 3213–3219.

Zhang, Q., et al. (2007b), Ubiquity and dominance of oxygenated species in organic aerosols in anthropogenically-influenced Northern Hemisphere midlatitudes. *Geophys. Res. Lett.*, *34*, L13801, doi:10.1029/2007GL029979.

Zhang, Q., J. L. Jimenez, M. R. Canagaratna, I. M. Ulbrich, N. L. Ng, D. R. Worsnop, and Y. L. Sun (2011), Understanding atmospheric organic aerosols via factor analysis of aerosol mass spectrometry: A review, *Anal. Bioanal. Chem.*, *401*(10), 3045–3067.

Zhang, X., A. Hecobian, M. Zheng, N. H. Frank, and R. J. Weber (2010), Biomass burning impact on PM(2.5) over the southeastern US during 2007: Integrating chemically speciated FRM filter measurements, MODIS fire counts and PMF analysis, *Atmos. Chem. Phys.*, *10*(14), 6839–6853.

Zhang, X., J. Liu, E. T. Parker, P. L. Hayes, J. L. Jimenez, J. A. de Gouw, J. H. Flynn, N. Grossberg, B. L. Lefer, and R. J. Weber (2012), On the gas-particle partitioning of soluble organic aerosol in two urban atmospheres with contrasting emissions: 1. Bulk water-soluble organic carbon, *J. Geophys. Res.*, *117*, D00V16, doi:10.1029/2012JD017908.

Zhuang, H., C. K. Chan, M. Fang, and A. S. Wexler (1999), Formation of nitrate and non-sea-salt sulfate on coarse particles, *Atmos. Environ.*, *33*(26), 4223–4233.